TRANSPORT MEASUREMENTS OF

SUPERCONDUCTOR

$Bi_{1.6}Pb_{0.4}Sr_2Ca_{2-x}Sm_xCu_3O_y$

by

Hüseyin AYDIN

AUGUST 2005

TRANSPORT MEASUREMENTS OF SUPERCONDUCTOR $Bi_{1.6}Pb_{0.4}Sr_2Ca_{2-x}Sm_xCu_3O_y$

by

Hüseyin AYDIN

THESIS SUBMITTED TO
THE GRADUATE SCHOOL OF NATURAL AND APPLIED SCIENCES
OF
THE ABANT İZZET BAYSAL UNIVERSITY
IN PARTIAL FULFILLMENT OF THE REQUIREMENTS FOR THE DEGREE
OF
MASTER OF SCIENCE
IN
THE DEPARTMENT OF PHYSICS

AUGUST 2005

Approval of the Graduate School of Natural and Applied Science

Prof. Dr. Davut KÖŞKER

Director

I certify that this thesis satisfies all the requirements as a thesis for the degree of Master of Science.

Prof. Dr. Ahmet Turan ALAN

Head of Physics Department

This is to certify that we have read this thesis and that in our opinion it is fully adequate, in scope and quality as a thesis for the degree of Master of Science.

Assist. Prof. Dr. Cabir TERZİOĞLU

Supervisor

Examining Committee Members

1. Assoc. Prof. Dr. Ahmet VARİLCİ ……
2. Assoc. Prof. Dr. Resul ERYİĞİT ……
3. Assist. Prof. Dr. Cabir TERZİOĞLU ……

ABSTRACT

TRANSPORT MEASUREMENTS OF

SUPERCONDUCTOR $Bi_{1.6}Pb_{0.4}Sr_2Ca_{2-x}Sm_xCu_3O_y$

Hüseyin AYDIN

Master of Science, Department of Physics

Supervisor: Assist. Prof. Dr. Cabir TERZİOĞLU

August 2005, 97 pages

We have investigated the effect of the partial substitutions of Ca by Sm in the Bi-2223 superconducting samples, which are prepared by standard solid-state

reaction methods. Magnetoresistivity measurements were made by using four-probe method with DC current of 10mA at 25-130 K temperature interval under constant magnetic field (0.0, 0.3, 0.6T). Electrical resistivity measurements were made by using four-probe methods with DC current of 10mA in the temperature range between 25-130 K. Hence, I-V and magnetic field as function of resistance measurements were done at constant temperatures (70,75, and 80K) under magnetic field which changes from 0.0 T to 0.6 T. Transition temperatures from superconducting state to normal state,Tc, critical current density Jc, activation energy U(H), irreversibility lines are determined from these measurements.

According to Arrhenius formula, which is given below;

$$\ln(\rho / \rho_0) = - \frac{U_0}{k_B T}$$

We obtain that U_0 is the slope of arrhenius plot to $\ln(\rho / \rho_0)$ versus 1/T as function of external field. We use linear fits to the apparently linear parts of the curves (in the resistivity parts) to extract activation energies, U_0, from the graph.

It is observed that the critical temperatures and the activation energies depend on both the Sm content of samples and the magnetic field. Increasing the Sm content shifted the irreversibility temperature to a lower temperature. The critical current density is decreased with increasing Sm content. The electrical resistivity is increased with increasing Sm content and increasing applied magnetic field. Hence, when magnetic field increased T_c^{onset} is same (this property of type II superconductors) T_c^{offset} value shifted to low temperature.

ÖZET

SÜPERİLETKEN $Bi_{1.6}Pb_{0.4}Sr_2Ca_{2-x}Sm_xCu_3O_y$ BİLEŞİĞİNİN TRANSPORT ÖLÇÜMLERİ

Hüseyin AYDIN

Yüksek Lisans, Fizik Bölümü

Tez Danışmanı: Yrd. Doc. Dr. Cabir Terzioğlu

Ağustos 2005, 97 sayfa

Ca yerine Sm katkısının etkileri Bi-2223 süperiletkenler katıhal yöntemiyle hazırlanmış örneklerde incelendi. 4 nokta yöntemi kullanılarak 10mA akım ve 25K-130K sıcaklıkları arasında elektriksel direnç ölçümleri yapıldı. 4 nokta yöntemi

kullanılarak 10mA akım ve 25K-130K sıcaklıkları arasında 0.0, 0.3,0.6T sabit magnetic alan altında magnetoresistivity ölçümleri yapıldı. Ayrıca, sabit sıcaklıklarda (70,75 ve 80K de) magnetic alanın direncin fonksiyonu ve I-V ölçümleri yapıldı.

$$\ln(\rho / \rho_0) = -\frac{U_0}{k_B T}$$

Şeklinde verilen Arrhenius formulü kullanılarak $\ln(\rho / \rho_0)$, 1 / T grafiğinin düşük özdirenç değerlerinde lineer davranış gösterdiği bölgenin eğiminden aktivasyon enerjisi hesaplandı.

Bu ölçümlerden, normal durumdan süperiletken duruma geçiş sıcaklığı T_c, kritik akım yoğunluğu J_c, aktivasyon enerjisi U(H), tersinmezlik çizgileri belirlendi. Kritik sıcaklık ve aktivasyon enerjisi, Sm katkısına ve magnetik alana bağlı olduğu görüldü. Sm katkısı arttıkça tersinmezlik sıcaklığı düşük sıcaklığa doğru kaydı. Sm katkısı ve magnetik alan arttıkça, kritik akım yoğunluğu azaldı. Ayrıca alan arttıkça T_c^{onset} değeri aynı olup (bu da II. Tip süperiletkenler özelliğidir.) T_c^{offset} değeri düşük sıcaklığa doğru kaydığı gözlendi.

To my parents…

ACKNOWLEDGMENTS

It is a great pleasure to thank many people who have contributed to the completion of this thesis through their knowledge, guidance, support and friendship. First of all, I would like to thank my thesis supervisor, Asst. Prof. Dr. Cabir TERZİOĞLU for his support, guidance, patience and encouragement during the preparation of this thesis. My understanding of physics has been improved by his enthusiasm and practical viewpoints. Moreover, he gave me many chances to meet impressive physicists and opportunities to discuss with them. I also, thank to Assistant Özgür ÖZTÜRK for many discussions, his assistances and enlightening comments on my works.

I am grateful to Associated Prof. Dr. Ahmet VARİLCİ and Associated. Prof. Dr. Resul Eryiğit along with my advisor for serving on my thesis committee.

I also acknowledge Assist. Prof. Dr. Mustafa YILMAZLAR for providing superconductor sample at Kırıkkale University.

Finally in my personal side I would like to thank my parents for their continuous supports, patience and encouragement which made it possible for me to continue my research.

TABLE OF CONTENTS

LIST OF TABLES

LIST OF FIGURES

CHAPTER 1

INTRODUCTION

The electrical resistivity of many metals and alloys drops suddenly to zero when they are cooled to low temperatures and they have no resistance value against current. This phenomena, that is called Superconductivity, was discovered by H. Kamerlingh Onnes in 1911 at University of Leiden. Onnes experimenting with platinum found that when cooled, its resistance fell to low value, which depended on the purity of the specimen. At that time the purest available metal was mercury and he observed no resistance in mercury when it was cooled to 4.2 K and then Onnes discovered that mercury is a superconductor at liquid helium temperature [1].

In 1933, one of the other surprising property of the superconductivity was discovered by Meissner and Ochsenfeld. According to this theory; a bulk superconductor in a weak magnetic field act as a perfect diamagnetic, with zero magnetic induction in the interior. When a specimen is placed in a magnetic field and is then cooled through the transition temperature for superconductivity, magnetic flux originally present is ejected from the specimen, this is called **Meissner Effect**. [2].

There were two problems to use of these two properties of superconductivity in the new technology. First one is the necessity of very low temperatures for superconductivity. We could supply this situation with using liquid helium but to produce liquid helium was so expensive in those years. Second one is the condition of superconductivity of any metal, when a magnetic field applied to, or current flowed through the specimen, superconductivity was corrupting so the pratical value was decreasing in applications.

Powerful magnets were made with using Nb-Ti which is a superconductor. Nb_3Ge Compound had the highest critical temperature in superconductors in 1973 (23 Kelvin).

In those years scientists dreamed to produce superconductors which are in the superconducting state at liquid nitrogen was easier and cheaper than producing liquid helium.

In 1986, Muller and Bednorz, who were working at IBM Zurih, found the critical temperature as 30 K for the compound La-Ba-Cu-O prepared by using barium oxide and cupper oxide [3]. This ceramic compound is the first high temperature superconductor. Its multiphase nominal compound has the formula of $La_{5x}Ba_xCu_5O_{5(3-y)}$. Its critical temperature changes with the change of x value. In $La_{2-x}Ba_xCuO_4$ compound, the highest T_c value for x=0.15 is obtained [4]. Then, by using strontium instead of barium, the value of T_c is raised to 36 K [5]. In addition, the crystal structure of this compound was found to be perovskite structure.

In1987, Wu Ashburn et al. found a new compound, Y-B-C-O, by using yttrium oxide instead of lanthanum oxide and the critical temperature was over 90 K [6]. This was really an important progress because a new sample which shows superconductivity in liquid nitrogen temperature and is easier to produce and cheaper

was found. The multiphase nominal compounds of this sample were $Y_{1.2}Ba_{0.3}Cu_2O_{4-x}$ and $Y_{0.6}Ba_{0.4}CuO_{3-x}$. Then, the scientists determined that the uniphase compound is $YBa_2Cu_3O_7$. By looking at the ratios of barium yttrium and copper, this compound is called as 1:2:3 or Y-B-C-O [7,8,9,10]. The newly found sample was in perovskite structure as in La-Ba-Cu-O compound. The difference between two compounds is oxygen vacancy. By means of those vacancies, there is the possibility of changing the critical temperature [11].

In 1987, a new chain is added to the superconductivity studies. Michael et al. found the superconductivity in Bi-Sr-Cu-O system [12]. In 1988, Maeda and his group observed superconductivity at 105 K by adding calcium to this system as Bi-Sr-Ca-Cu-O [13]. Also Tokano and his group found a stable superconductor at 110 K, by adding lead to the system [14]. Addition of lead increases the ratio of the phase which has high critical temperature. In 1992, Quidwai and his group observed the transition to superconductivity at 130-140 K by adding antimony to the system [15].

In 1988, Sheng and Parkin observed superconductivity in Tl-Ba-Ca-Cu-O compound first at 110 K and then at 125 K. But this compound has cancerogenic effect and was not stable and it has to be produced each time. During these passing years, studies on different samples went on. In 1993, Schilling and his group observed superconductivity in $HgBa_2Ca_2Cu_3O_{1+x}$ compound at 133 K and Chu and his group observed superconductivity in high pressure with Hg based compounds at 150 K [16].

In 2001, J.Nagamatsu, J.Akimitsu and their group observed superconductivity in MgB_2 compound at 39 K [17]. This was a very important improvement in Type I superconductors. Although the sample was a type-I its critical temperature was quite

high. And since it was elastic, it had the advantage of being easy to be adapted to technology. Studies on this system are going on and it is still popular.

For many years it was thought that all superconductors behaved according to a basically similar pattern. However, it is now realized that there are two kinds of superconductor, which are known as type-I and type-II superconductivity, where as alloys generally exhibit type-II superconductivity. The two types have many properties in common but show considerable differences in their magnetic behavior. These differences are sufficient for us to treat the two types separately.

The aim of this study is to prepare Bi-Pb-Sr-Ca-Cu-O samples, to investigate the physical and microstructure properties of the BSCCO by performing DC resistivity, critical current, XRD measurements, and to compare the outputs with other experimental results.

Chapter II gives the physical properties of superconductivity, chapter III gives a review of high temperature superconductors, chapter IV gives crystal structure of the Bi-based system, chapter V gives experimental procedure, and chapter VI gives the results and discussion. The last chapter gives the conclusion of the work in this dissertation.

CHAPTER II

THE PHYSICAL PROPERTIES OF SUPERCONDUCTIVITY

2.1 Introduction

The electrical resistivity of all metals and alloys drops suddenly to zero when they are cooled to sufficiently low temperature, often a temperature in the liquid helium range [1]. The current in a conductor is carried by "conduction electrons" which are free to move through the material. Electrons have, of course, a wave-like nature, and an electron travelling through a metal can be represented by a plane wave progressing in the same direction. A metal has a crystalline structure with the atoms lying on a regular repetitive lattice, and it is a property of a plane wave that it can pass through a perfectly periodic structure without being scattered into other directions. Hence an electron is able to pass through a perfect crystal without any loss of momentum in its original direction. However, any fault in the periodicity of the crystal will scatter the electron wave and introduce some resistance. There are two effects which can spoil the perfect periodicity of a crystal lattice and so introduce resistance. At temperatures above absolute zero the atoms

are vibrating and will be displaced by various amounts from their equilibrium positions; furthermore, foreign atoms or other defects randomly distributed can interrupt the perfect periodicity. Both the thermal vibrations and any impurities or imperfections scatter the moving conduction electrons and give rise to electrical resistance [18].

We can understand why the electrical resistivity decreases when a metal or alloy is cooled. When the temperature is lowered, the thermal vibrations of the atoms decrease and the conduction electrons are less frequently scattered. The decrease of resistance is linear down to a temperature equal to about one-third of the characteristic Debye temperature of the material, but well below this the resistivity varies as T^5.For a perfectly pure metal, therefore, where the electron motion is impeded only by the thermal vibrations of the lattice, the resistivity should approach zero as the temperature is reduced towards 0 K. Any real specimen of metal cannot be perfectly pure and will contain some impurities. Therefore the electrons, in addition to being scattered by thermal vibrations of the lattice atoms, are scattered by the impurities, and this impurity scattering is more or less independent of temperature. As a result, there is a certain "residual resistivity"' (ρ_0, Fig. 2.1) which remains even at the lowest temperatures. The more impure the metal, the larger will be its residual resistivity.

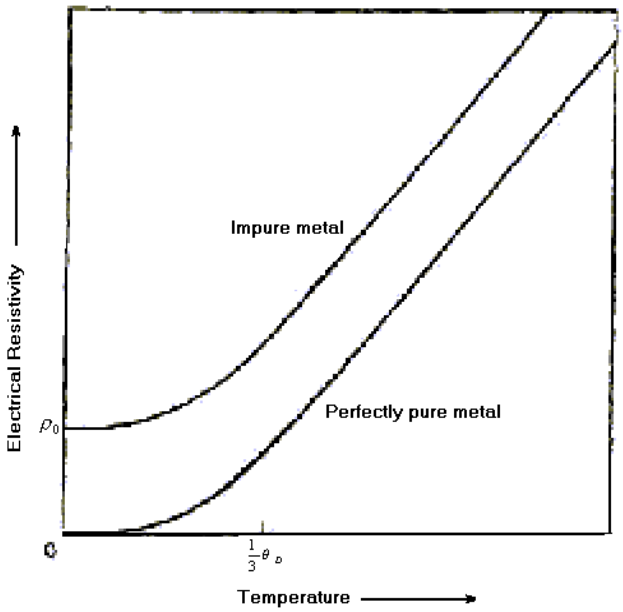

Figure 2.1. Variation of resistance of metals with temperature.

Certain metals, however, show a very remarkable behavior; when they are cooled their electrical resistance decreases in the usual way, but on reaching a temperature a few degrees above absolute zero they suddenly lose all trace of electrical resistance (Fig. 2.2). They are then said to have passed into the superconducting state. The transformation to the superconducting state may occur even if the metal is so impure that it would otherwise have had a large residual resistivity [18].

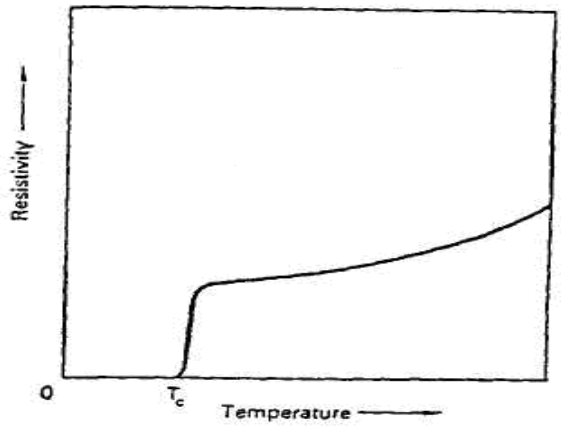

Figure 2.2. Loss of resistance of a superconductor at low temperatures.

Table 2.1. Superconducting Elements.

H																	He
Li	Be											B	C	N	O	F	Ne
Na	Mg											Al	Si	P	S	Cl	Ar
K	Ca	Sc	Ti	V	Cr	Mn	Fa	Co	Ni	Cu	Zn	Ga	Ge	As	Se	Br	Kr
Rb	Sr	Y	Zr	Nb	Mo	Tc	Ru	Rh	Pd	Ag	Cd	In	Sn	Sb	Te	I	Xe
Cs	Ba	Lu	Hf	Ta	W	Re	Os	Ir	Pt	Au	Hg	Tl	Pb	Bi	Po	At	Rn
Fr	Ra																

La	Ca	Pr	Nd	Pm	Sm	Eu	Gd	Tb	Dy	Ho	Er	Tm	Yb
Ac	Th	Pa	U	Np	Pu								

Si Superconducting under high pressure or in thin films

Al Superconducting

Li Metallic but not yet found to be superconducting

2.2 Superconducting Transition Temperature

The transition to the superconducting state is a sharp one in bulk specimens. Above a critical temperature T_c the properties of the metal are completely normal; below T_c superconducting properties are displayed, the most dramatic of which is the absence of any measurable DC electrical resistance. Measured critical temperatures range from a few millidegrees Kelvin up to a little over 20 K. The corresponding thermal energy $k_B T_c$ varies from about 10^7 eV up to a few thousandths of an electron volt. This is quite minute compared with the energies we have become accustomed to regarding as significant in solids [19]. Transition temperatures of the superconducting elements are listed in Table 2.2.

Table 2.2. Values of T_c and H_c for the Superconducting Elements

ELEMENT		T_c (K)	H_c (GAUSS)[b]
Al		1.196	99
Cd		0.56	30
Ga		1.091	51
Hf		0.09	—
Hg	α (rhomb)	4.15	411
	β	3.95	339
In		3.40	293
Ir		0.14	19
La	α (hcp)	4.9	798
	β (fcc)	6.06	1096
Mo		0.92	98
Nb		9.26	1980
Os		0.655	65
Pa		1.4	—
Pb		7.19	803
Re		1.698	198
Ru		0.49	66
Sn		3.72	305
Ta		4.48	830
Tc		7.77	1410
Th		1.368	162
Ti		0.39	100
Tl		2.39	171
U	α	0.68	—
	γ	1.80	—
V		5.30	1020
W		0.012	1
Zn		0.875	53
Zr		0.65	47

Niobium is the metallic element with the highest transition temperature (9.3 K), but some alloys and metallic compounds remain superconducting up to even higher temperatures. For example; Nb_3Sn has a transition temperature of just over 18 K. In general, the transition temperature is not very sensitive to small amounts of impurity, but the superconductivity of a few metals, such as iridium and molybdenum, which in the pure state have very *low* transition temperatures, may be destroyed by the presence of minute quantities of magnetic impurities. Such elements, therefore, only exhibit superconductivity if they are extremely pure, and specimens of these metals of normal commercial purity are not superconductors.

On cooling, the transition to the superconducting state may extremely sharp if the specimen is pure and physically perfect example, in a good gallium specimen the transition has been observed to occur within a temperature range of 10^{-5} degrees.

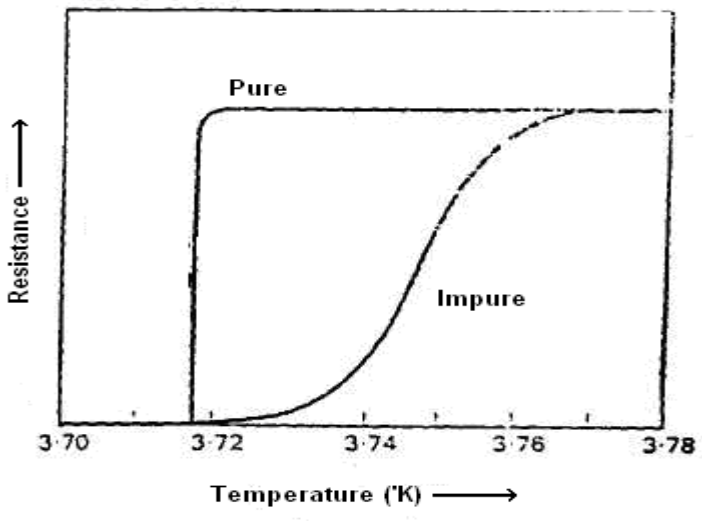

Figure 2.3. Superconducting transition in tin.

If however, the specimen is impure or has a disturbed crystal structure, the transition may be considerably broadened. Figure 2.3 shows the transition in purer and impure tin specimens [18].

2.3 Zero Resistance

Even when the transition is spread over a considerable temperature range the resistance still seems to disappear completely below a certain temperature. We naturally ask whether in the superconducting state the resistance has indeed become zero or whether it has merely fallen to a very small value. Of course, it can never be proved by experiment that the resistance is in fact zero; the resistance of any specimen may always be just less than the sensitivity of our apparatus allows us to detect. However, no experiment has been able to detect any resistance in the superconducting state. We may look for resistance quite simply bypassing a current through a wire of superconductor and seeing if any voltage is recorded by a sensitive voltmeter connected across the ends of the wire. A more sensitive test, however, is to start a current flowing round a closed superconducting ring and then see whether there is any decay in the current after a long period of time. Suppose the self-inductance of the ring is *L;* then, if at time $t = 0$ we start a current I(0) flowing round the ring at a later time *t* the current will have decayed to

$$i(t) = i(0)e^{-(R/L)t} \qquad (2.1)$$

where R is the resistance of the ring. We cannot put an ammeter into the circuit to measure the current but we can measure the magnetic field that the circulating current produces and see if this decays with time. The measurement of the magnetic field does not draw energy from the circuit, and we should be able to observe whether the current circulates indefinitely. As can be seen from Eq.2.1, the smaller the inductance L of the circuit the more rapid the decay of current for a given value of resistance R and the more sensitive experiment [18].

2.4 Critical Currents

The early workers in superconductivity soon discovered that there is an upper limit to the amount of current that can be passed along a piece of superconductor if it is to remain resistanceless. We call this the critical current of that particular piece. If the current exceeds this critical value, resistance appears.

We now show that the critical current is related to the critical magnetic field strength H_c. We saw that all currents in a superconductor flow at the surface within the penetration depth, the current density decreasing from some value J_a at the surface. It was pointed out in previous that superconductivity breaks down if the supercurrent density exceeds a certain value which we call the critical current density J_c.

In general there can be two contributions to the current flowing on the surface of a superconductor. Consider, for example, a superconducting wire along which we are passing a current from some external source such as a battery. We call this current the transport current because it transports charge into and out of the

wire. If the wire is in an applied magnetic field, screening currents circulate so as to cancel the flux inside the metal. These screening currents are superimposed on the transport current, and at any point the current density J can be considered to be the sum of a component J_i due to the transport current and a component J_H which arises from the screening currents

$$J = J_{i} + J_H \tag{2.2}$$

We may expect that superconductivity will break down if the magnitude of the total current density J at any point exceeds the critical current density J_c. According to the London equation, there is a relation between tne supercurrent density at any point and the magnetic flux density at that point, and this same relation holds whether the supercurrent is a screening current, a transport current or a combination of both. Hence, when a current flows on a superconductor, there will at the surface be a flux density B and a corresponding field strength $H\left(= B/\mu_0\right)$ which is related to the surface current-density J_a.

A superconductor loses its zero resistance when, at any point on the surface, the total magnetic field strength, due to transport current and applied magnetic field, exceeds the critical field strength H_c. Clearly the stronger the applied magnetic field the smaller is this critical current.

If there is no applied magnetic field the only magnetic field will be that generated by any transport current, so in this case, the critical current will be that current which generates the critical magnetic field strength H_c at the surface of the conductor. This special case of the general rule stated above is known as Silsbee's hypothesis and was formulated before the concept of critical current density was

appreciated. We shall call the more general rule for the critical current given in the previous paragraph the "generalized form" of Silsbee's hypothesis.

The general form of Silsbee's Rule states that resistance first appears when the total magnetic field strength at any part of the surface equals H_c , and so the critical current in this case is given by;

$$i_c = 2\pi a(H_c - 2H_a) \tag{2.3}$$

In this case, therefore, the critical current decreases linearly with increase in applied field strength, falling to zero at $\frac{1}{2}H_c$. The critical magnetic field strength H_c depends on the temperature, decreasing as the temperature is raised and falling to zero at the transition temperature T_c. This implies that the critical current density depends on temperature in a similar manner, the critical current density decreasing at higher temperatures. Conversely, if a superconductor is carrying a current, its transition temperature is lowered [18].

2.5 PERFECT DIAMAGNETISM

2.5.1. Magnetic Properties of a Perfect Conductor

A superconductor below its transition temperature appears to have no resistance. Suppose that we cool a specimen, which below its transition temperature, becomes perfectly conducting. The resistance around an imaginary closed path within

the metal is zero; and therefore, the amount of magnetic flux enclosed within this path cannot change. This is true for any such imaginary circuit and this can only be so if the flux density at every point within the metal does not vary with time, i.e.

$$B = 0. \tag{2.4}$$

Consequently the flux distribution in the metal must remain, as it was when the metal became resistanceless.

Consider now the behaviour of a perfect conductor under various circumstances. Suppose that a specimen loses its resistance in the absence of any magnetic field and that a magnetic field is then subsequently applied. Because the flux density in the metal cannot change, it must remain zero even after the application of the magnetic field. In fact the application of the magnetic field induces resistanceless currents which circulate on the surface of the specimen in such a manner as to create a magnetic flux density which everywhere inside the metal is exactly equal and opposite to the flux density of the applied magnetic field, Because these currents *do* not die away, the net flux density inside the material remains at zero. This is illustrated in Fig. 2.4a: the surface currents *i* generate a flux density B that exactly cancels the flux density B_a of the applied magnetic field everywhere inside the metal. These surface currents are often referred to as screening currents.

The flux density created by the persistent surface currents does not. of course, disappear at the boundary of the specimen, but the flux lines form continuous closed curves which return through the space outside (Fig. 2.4a).

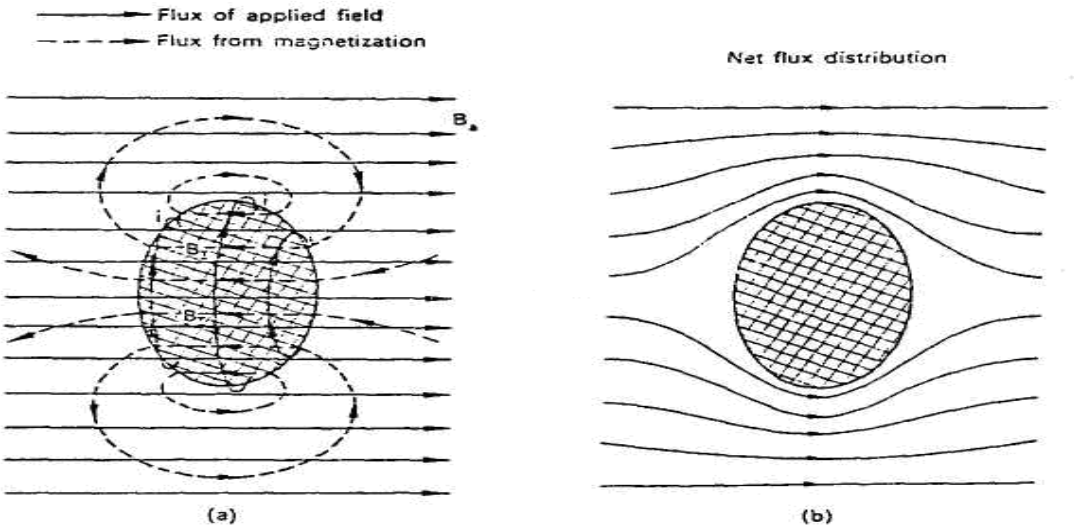

Figure 2.4. Distribution of magnetic flux about a perfectly diamagnetic body.

Though the density of this flux everywhere *inside,* the specimen is equal and opposite to the flux from the applied field, this is not so *outside* the specimen. The net distribution of flux resulting from the superposition of the flux from the specimen and that from the applied field is shown in Fig. 2.4b. The pattern is as though the sample had prevented entry into it of the flux of the applied field. A sample in which there is no net flux density when a magnetic field is applied is said to exhibit perfect diamagnetism. If we now reduce the applied magnetic field to zero the specimen is left in its original unmagnetized condition. The above sequence of events is illustrated in Fig. 2.5 a-d.

Let us now consider a different sequence of events. Suppose that the magnetic field B_a is applied to the specimen while it is above its transition temperature (Fig. 2.5e). Most metals (other than the special ferromagnetics, iron, cobalt and nickel)

have values of relative magnetic permeability very close to unity, and so the flux density inside is virtually the same as that of the applied field.

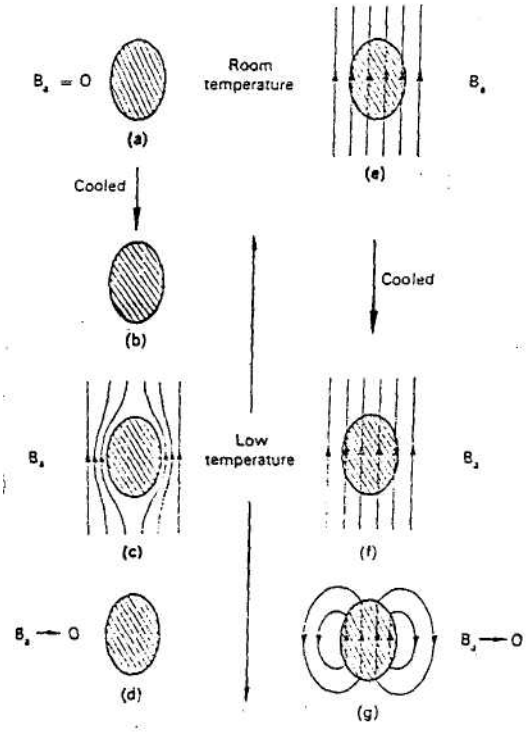

Figure 2.5. Magnetic behaviour of a "perfect" conductor, (a)-(b) Specimen becomes resistanceless ia absence of field, (c) Magnetic field applied to resistanceless specimen, (d) Magnetic field removed.(e)-(f) Specimen Kvomts resistanceless in applied magnetic field, (g) Applied magnetic field removed.

The specimen is now cooled to a low temperature so that it loses its electrical resistance. This disappearance of resistance has no effect on the magnetization, and the flux distribution remains unaltered (Fig. 2.5f). We next reduce the applied field to zero. The flux density inside the perfectly conducting metal cannot change, and persistent currents are induced on the specimen, maintaining the flux inside, with the result that the specimen is left permanently magnetized (Fig. 2.5g). It is important to notice that in (c) and (f) of Fig. 2.5 the sample is under the same conditions of temperature and applied magnetic field. And yet its state of magnetization is quite

different in the two cases. Similarly (d) and (g) show different states of magnetization under identical external conditions. We see that the state of magnetization of a perfect conductor is not uniquely determined by the external conditions but depends on the sequence by which these conditions were arrived at [18].

2.6 Special Magnetic Behaviour of a Superconductor

2.6.1 Meissner effect

A magnetic field (provided that it is not too strong) cannot penetrate into the interior of a superconductor. This is most dramatically illustrated by the Meissner-Ochsenfeld effect: If a normal metal in a magnetic field is cooled below its superconducting transition temperature, the magnetic flux is abruptly expelled. Thus the transition, when it occurs in a magnetic field, is accompanied by the appearance of whatever surface currents are required to cancel the magnetic field in the interior of the specimen [19]. They found that the expected situation of Fig.2.5f did not in fact occur, but that at their transition temperatures the specimens spontaneously became perfectly diamagnetic, cancelling all flux inside, as in Fig. 2.5c, even though they had been cooled in a magnetic field. This experiment was the first to demonstrate that superconductors are something more than materials which are perfectly conducting; they have an additional property that a merely resistanceless metal would not possess: a metal in the superconducting state never allows a magnetic flux density to exist in its interior.

That is to say, inside a superconducting metal we always have B=0. Where as inside a merely resistanceless metal there may or may not be a flux density, depending on circumstance (Fig. 2.5). When a superconducting cooled in a weak magnetic field at the transition temperature persistent currents arise on the surface and circulate so as to cancel the flux density inside, in just the same way as/when a magnetic field is applied after the metal has been cooled (Fig. 2.6). This effect, where by V superconductor never has a flux density inside even when in an applied magnetic field, is called (within justice to Ochsenfeld) the Meissner effect.

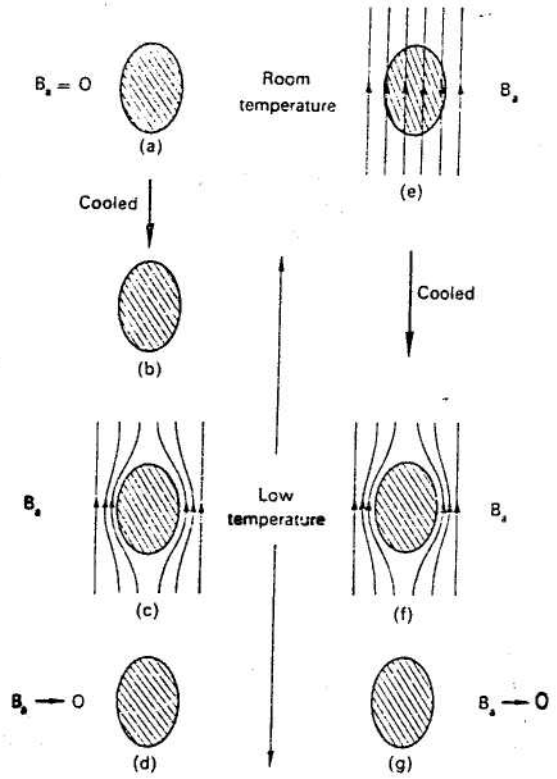

Figure 2.6. Magnetic behaviour of a superconductor, (a)-(b) Specimen becomes resistanceless in absence of magnetic field, (c) Magnetic field applied to superconducting specimen, (d) Magnetic field removed. (e)-(f) Specimen becomes superconducting in applied magnetic field, (g) Applied magnetic field removed.

For convenience we call a hypothetical metal which simply has no resistance and would behave as shown in Fig. 2.5a '"perfect conductor" in contrast to superconductors which in the superconducting state never permit a magnetic flux density to exist inside them (Fig. 2.6). The state of magnetization of a "perfect conductor" would depend on the order in which the final conditions of applied magnetic field and temperature were obtained, but the magnetization of a superconductor depends only on the actual values of the applied field and temperature and not on the way they were arrived at [18].

2.7. Surface Currents

The fact that a superconducting metal does not allow magnetic flux to exist in its interior has an important effect on any electric currents that flow along it; currents cannot pass through the, body of a superconducting metal, but flow only on the surface. At any point in a material of unit relative permeability the relation between the magnetic flux and current density is, from Maxwell's equation.

$$curlB = \mu_0 J \qquad (2.5)$$

If the metal is superconducting B is zero inside, and so curl B must also be zero inside. It follows, therefore, from Maxwell's equation that,

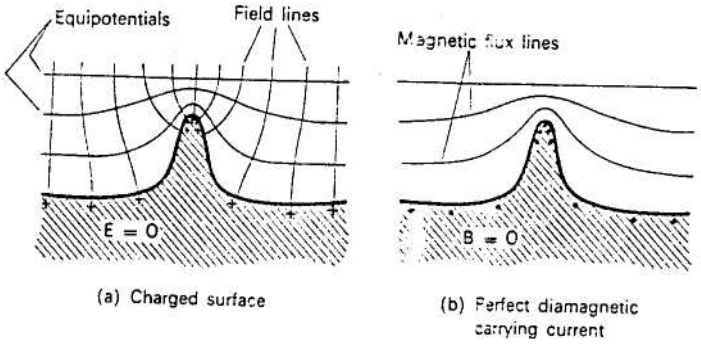

Figure 2.7. Analogy between distribution of electrostatic charge and surface current. + + + electric charges . . . current perpendicular to plane of page.

as a consequence of B being zero, the current density J must also be zero within the superconductor. There is, of course, no reason *why* B must be zero outside the superconductor so, if there is a current, it flows not through the metal but on the surface. This is true both of currents passed along the superconductor from some external source such as a battery (we call these "transport" currents), and of diamagnetic screening currents. Any transport current will flow all over the surface, creating a magnetic flux outside but not inside the conductor. If a magnetic field is applied, the diamagnetic screening currents, which flow so as to cancel the flux density inside also circulate on the surface. There is an interesting and useful analogy between the distribution of current on the surface of a superconducting metal and the distribution of electrostatic charge on a conducting body. Consider part of the surface of a charged conductor as shown in Fig. 2.7a. In the equilibrium state $E = 0$ inside the conductor but, if the body carries a surface charge, this charge will produce an electric field outside the conductor The component of the electric field parallel to the surface, E_{II}, is continuous across the surface and therefore, since $E = 0$ in the conductor, E_{II} must be zero just outside the surface. The electric field lines must consequently meet the conductor at right angles. The

surface itself is an equipotential and the electric field lines are orthogonal to the equipotentials. It can be seen that the field lines are crowded together where the boundary has a high convex curvature, so the electric charge, being proportional to the normal component of the field, will be concentrated into these regions. Figure 2.4b shows a section of part of a superconducting metal carrying a current in a direction normal to the plane of the paper. Inside the perfectly diamagnetic material we have $B = 0$, but if current is flowing on the surface there will be a magnetic flux density outside. The component of B normal to the surface is continuous across the boundary, so just outside the surface the flux lines must be parallel to the surface. This flux density is proportional to the surface current density. In fact the external magnetic field due to the surface current has the same form as the equipotentials due to surface charges in Fig.2.7a. The magnetic field lines are crowded together close to the region where the surface has high convex curvature, so the surface current density must be greatest at these regions. We might expect, therefore, that the distribution of surface current on a perfectly diamagnetic body has the same form as the distribution of electric charge on a charged conductor of the same shape, and a proper mathematical analysis shows that this is indeed so [18].

2.8 The London Equation

F. London and H.London first examined in quantitive way the fundamental fact that a metal in the superconducting state permits no magnetic field in its interior. Their analysis start with the two-fluid

model of Gorter and Casimir. The only crucial assumption of this model that we shall use is that in a superconductor at temperature $T<T_c$, only a fraction $n_s(T)/n$ of the total number of conduction electrons are capable of participating in a supercurrent. The quantity $n_s(T)$ is known as the density of superconducting electrons. It approaches the full electronic density n as T falls well below T_c, but it drops to zero as T rises to T_c . The remaining fraction of electrons is assumed to constitute a "normal fluid" of density $n- n_s$ that cannot carry an electric current without normal dissipation. The normal current and the supercurrent are assumed to flow in parallel; since the later flows with no resistance whatever, it will carry the entire current induced by any small transitory electric field, and the normal electrons will remain quite inert. Normal electrons are therefore ignored in the diffusion that follows.

Suppose that an electric field momentarily arises within a superconductor. The superconducting electrons will be freely accelerated without dissipation so that their mean velocity v_s will satisfy

$$m\frac{dv_s}{dt} = -eE. \tag{2.6}$$

Since the current density carried by these electrons is $j = -ev_s n_s$, and then

$$\frac{d}{dt} j = \frac{n_s e^2}{m} E. \tag{2.7}$$

Note that the Fourier transform of above equation gives the ordinary AC conductivity for an electron gas of density n_s in the Drude model, when the relaxation time τ becomes infinitely large:

$$j(w) = \sigma(w)E(w),$$
$$\sigma(w) = i\frac{n_s e^2}{mw}. \tag{2.8}$$

Substituting 2(2.8) into Faraday's law of induction,

$$\nabla \times E = -\frac{1}{c}\frac{\partial B}{\partial t}, \tag{2.9}$$

gives the following relation between current density and magnetic field:

$$\frac{\partial}{\partial t}(\nabla \times j + \frac{n_s e^2}{mc} B) = 0. \tag{2.10}$$

This relation, together with Maxwell equation

$$\nabla \times B = \frac{4\pi}{c} j, \tag{2.11}$$

determines the magnetic fields and current densities that can exist within a perfect conductor.

Note in particular that any static field B determines a static current density j through Eq.2.10 since any time independent B and j are trivially solutions to Eq.2.9, the two equations are consistent with an arbitrary static magnetic field. This is incompatible with the observed behavior of superconductors, which permit no fields in their interior. F. London and H. London discovered that this characteristic behavior of superconductors could be obtained by restricting the full set of solutions of 4 to those that obey

$$\nabla \times j = -\frac{n_s e^2}{mc} B, \tag{2.12}$$

which is known as the London equation. London Equation specifically characterizes superconductors and distinguishes them from mere "perfect conductors," requires in addition that the time-independent value be zero [19].

2.9 Penetration Depth

Magnetic fields are expelled from the interior of a type I superconductor by the formation of surface currents. In reality, these currents are not formed in an infinitesimally thin layer on the surface. Instead, they penetrate the surface to a

small extent. Within this thin layer, which is about 100 nm in depth, the magnetic field *B* inside a type I superconductor decreases exponentially from its external value to zero according to the expression

$$B(x) = B_0 e^{-x/\lambda} \tag{2.13}$$

where it is assumed that the external magnetic field is parallel to the surface of the sample. In this equation, B_o is the value of the magnetic field at the surface, x is the distance from the surface to some interior point, and λ is a parameter called the penetration depth. The variation of the magnetic field inside a semi-infinite type I superconductor with distance is plotted in Figure 2.8. The superconductor occupies the region on the positive side of the *x-axis*. As you can see, the magnetic field becomes very small at depths a few times λ below the surface. Values for λ are typically in the range of 10-100 nm.

The penetration depth varies with temperature according to the empirical expression

$$\lambda(T) = \lambda_0 \left[1 - \left(\frac{T}{T_c} \right)^2 \right]^{-1/2} \tag{2.14}$$

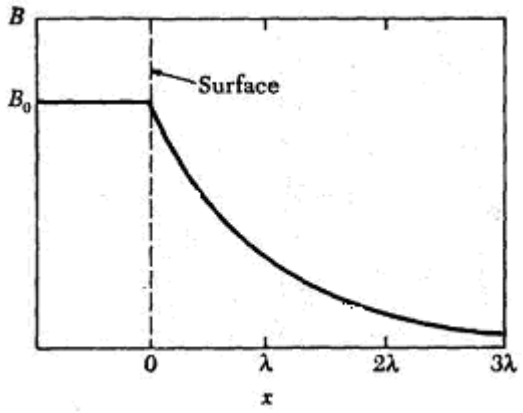

Figure 2.8. The magnetic field *B* inside a semi-infinite superconductor versus distance i from its surface. The field outside the superconductor (for x < 0) is B_o, and the superconductor is to the right of the dashed line.

where λ_o is the penetration depth at T = 0 K. From this we see that λ becomes infinite as T approaches T_c. Furthermore, as T approaches T_c, while the sample is in the superconducting state, an applied magnetic field penetrates deeper into the sample. Ultimately, the field penetrates the entire sample (λ becomes infinite), and the sample becomes normal.

The existence of field penetration is especially important when dealing with type I superconductors in the form of thin films or small particles. For example, if the thickness of the film is comparable to or less than λ, an applied field would penetrate the sample and flux expulsion would not be complete [20].

2.9.1 Variation with temperature

The penetration depth does not have a fixed value but varies with temperature, as shown in Fig. 2.9. At low temperatures it is nearly independent of temperature and has a value λ_0 characteristic of the particular metal.

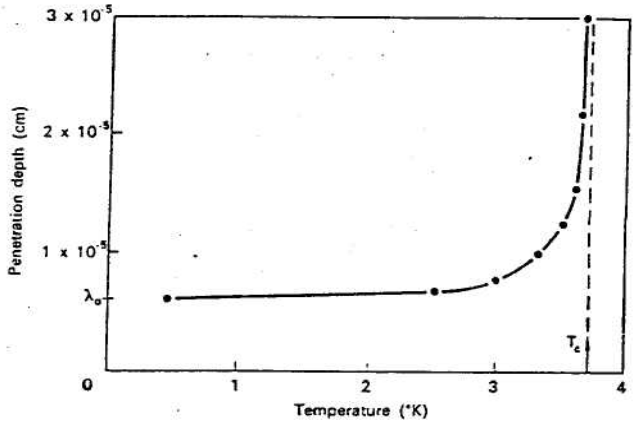

Figure 2.9 Variation with temperature of penetration depth in tin(after Schawlow and Devlin).

Above about 0-8 of the transition temperature, however, the penetration depth increases rapidly and approaches infinity as the temperature approaches the transition temperature.

The variation of Penetration depth with temperature is found to fit very closely the relation

$$\lambda = \frac{\lambda_0}{(1-t^4)^i} \qquad (2.15)$$

where t is the temperature relative to The transition temperature, $t = T/T_c$

Perfect diamagnetism does not, therefore, occur in specimens, which are very close to their transition temperature. The decrease in penetration depth is, however, so rapid as the temperature falls below T_c that any large departure from perfect diamagnetism would be extremely difficult to detect in bulk specimens because of the difficulty of holding the temperature sufficiently constant during a

measurement. For example, to observe a penetration depth of about 1 mm a specimen would, which is shown in above formula, have to be held at a temperature only 10^{-7} per cent below the transition temperature. In one experimental arrangement a rod of pure superconductor is surrounded by a closely fitting solenoid. When the temperature of the metal is lowered so that it becomes superconducting there can be no magnetic flux in the metal, except just below the surface within the penetration depth. Because the solenoid fits the rod very closely, its self-inductance largely dependent on the magnitude of this penetration depth [18].

2.10 Coherence Length

Another important parameter associated with superconductivity is called the coherence length, ξ. One can think of the coherence length as the smallest dimension over which superconductivity can be established or destroyed. Alternatively, one can view the coherence length as the distance over which the electrons in a Cooper pair remain together. In the BCS theory, the coherence length is directly related to the distance over which the two electrons in a Cooper pair remain correlated. Typical values of λ and ξ at T = 0 K for selected superconductors are given in Table 2.3.

A superconductor will be type I if the coherence length is larger than the penetration depth, λ. Most pure metals fall into this category. On the other hand, an increase in the ratio λ/ξ favors type II superconductivity. A detailed analysis

shows that the coherence length and penetration depth depend on the mean free path of the electrons in the normal state.

Table 2.3. Penetration Depth and Coherence Length of Selected Superconductors at $T = 0$ K

Superconductor	λ (nm)	ξ (nm)
Al	16	160
Cd	110	760
Pb	37	83
Nb	39	38
Sn	34	23

The mean free path of a metal can be reduced by adding impurities to the metal. As impurities are added to a metal, the penetration depth increases while the coherence length decreases. Thus, one can cause a metal to change from type I to type II by introducing another alloying element. For example, pure lead is a type I superconductor. However, it changes to a type II superconductor (with almost no change in T_c) by alloying it with 2% (by weight) of indium [20].

2.11 The Intermediate State

In previous sections about the critical field, we said that the flux was expelled by a superconductor until a field H_c was reached, whereupon the whole specimen made a discontinuous transition into the normal state. Actually, however, the transition is discontinuous only for specimens with simple geometries and particular field orientations: for example, a cylinder whose axis is oriented parallel to the field. Consider, on the other hand, the case in which the axis of the cylinder is normal to the field. Figure 2.10 shows the distribution of the field in the neighborhood

of the cylinder. The field is stronger at the points AA' than at the points DD' because of the "crowding" of the field lines at points AA'. It can be shown, in fact, that the AA' field is twice as strong as the DD' one. Thus as the intensity of the field is raised, it reaches its critical value at the points A A' before it does at DD', and the sides of the cylinder thus turn into a normal state at the field $H = \frac{1}{2} H_c$. As the intensity of the field is raised further, the specimen divides into alternate normal and superconducting laminae parallel to the field, as shown in Fig. 2.10., and the specimen is said to be in the intermediate state. And when the intensity of the field is raised still further, the normal regions grow until, at $H = H_c$. the whole specimen becomes completely normal.

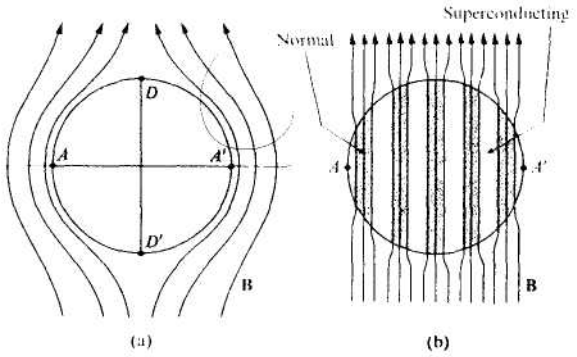

Figure 2.10. Intermediate state in a cylinder whose axis is normal to the field: (a) The situation for H<H_c /2. (b) The situation for $\frac{1}{2} H_c < H < H_c$, showing the intermediate state.

Because of the division into thin laminae, the field distribution is "straightened out." which leads to a reduction in the demagnetization energy of the superconducting regions, i.e., essentially the whole flux passes through the

normal region. The number of laminae, however, is kept finite by virtue of the fact that there is a surface energy associated with the wall between the superconducting and normal regions [21].

2.12 The Mixed State

The occurrence of this perfect diamagnetism implies the existence of a surface energy at the boundary between any normal and superconducting regions in the metal. This surface energy plays a very important role in determining the behaviour of a superconductor as type-I or a tvpe-II.

Consider a superconducting body in an applied magnetic field of strength less than the critical value H_c, and suppose that within the material a normal region were to appear with boundaries lying parallel to the direction of the applied magnetic field. The appearance of such a normal region would change the free energy of the superconductor, and we may consider two contributions to this free energy change: a contribution arising from the bulk of the normal region and a contribution due to its surface. An applied magnetic field of strength H_a, the free energy per unit volume of the normal state is greater than that of the superconducting, perfectly diamagnetic, state by an amount $\frac{1}{2}\mu_0(H_c^2 + H_a^2)$. Furthermore, there is a surface energy associated with the boundary between a normal and superconducting region. For the type-I superconductors we considered in the previous sections this surface energy is positive. Hence, if a normal region were to form in the superconducting material, there would be an increase in free energy due both to the bulk and to the surface of the

normal region. For this reason, the appearance of normal regions is energetically unfavorable, and a type-I superconductor remains superconducting throughout then a magnetic field of strength less than *H,* is applied.

Suppose, however, that in certain metals the surface energy between normal and superconducting regions were *negative* instead of positive (i.e. energy is released when the. interface, is formed). In this case the appearance of a normal region would, reduce the free energy, if the increase in energy due to the bulk of the region were outweighed by the decrease due to its surface. A material assumes that condition which has the lowest total free energy, so in the case of a sufficiently negative surface energy we would expect that, in order to produce the minimum free energy; a large number of normal regions would form in the superconducting material when a magnetic field is applied. The material would split into some fine-scale mixture of superconducting and normal *regions* whose boundaries lie parallel to the applied field, the arrangement being such as to give the maximum boundary area relative to volume of the material. We shall call this the *mixed state.* In the n section it will be shown that the conditions in some superconductors are such that the surface energy is indeed negative. These metals are therefore able to go into the mixed state, and these are the type-II superconductors.

It is important to distinguish clearly between the *mixed state,* which occurs in type-II superconductors and the *intermediate* state, which occurs in type-I superconductors. The intermediate state occurs in those type-I superconducting bodies, which have a non-zero demagnetizing factor, and its appearance depends on the shape of the body. The mixed state, however, is an intrinsic feature of type-II superconducting material and appears even if the body has zero demagnetizing factor (e.g. a long rod in a parallel field). In addition, the structure of the

intermediate state is relatively coarse and the gross features can be made visible to the naked eye. The structure of the mixed state is, as we shall see, on a much finer scale with a periodicity less than 10^{-5} cm [18].

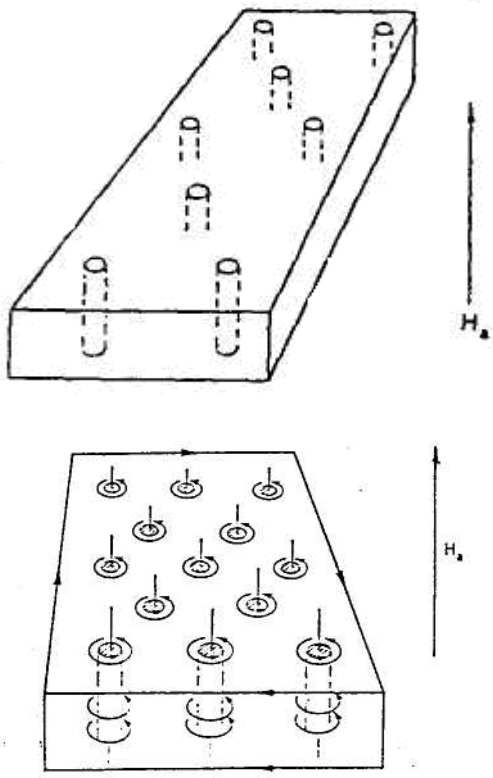

Figure 2.11. The mixed state, showing normal cores and encircling super-current vortices. The vertical lines represent the flux threading the cores. The surface current maintains the bulk diamagnetism.

2.13 Surface Energy

As a result of the existence of the penetration depth and coherence length, there is a surface energy associated with the boundary between a normal and superconducting region. It was shown that, if the coherence range is *longer* than the

penetration depth, as it is in most pure metallic elements, the total free energy is increased close to the boundary, that is to say there is a positive surface energy.

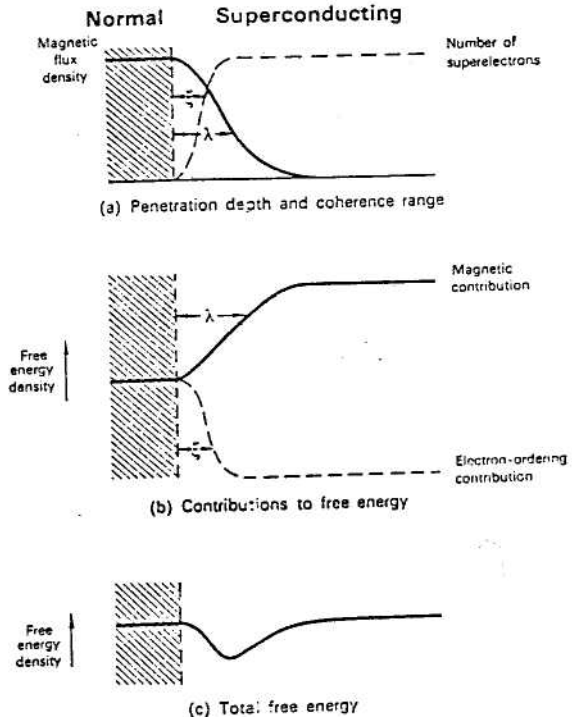

Fig 2.12. Negative surface energy, coherence range less than penetration depth.

The relative values of the coherence length ξ; and the penetration depth λ vary for different materials. In many alloys and a few pure metals the coherence range is greatly reduced, as was pointed out in previous sections. If the coherence length is *shorter* than the penetration depth, the surface energy is *negative,* as Fig. 2.12 (a) illustrates, and therefore such a superconductor will be type-II. In most pure metals the coherence length has a value *Co* of about 10^{-4} cm. This is considerably greater than the penetration depth, which is about 5×10^{-6} cm. so in such metals the surface energy is positive and they are type-I. It was pointed out in previous works that the coherence length is reduced if the electron mean free path is shortened;

consequently, the coherence length is reduced in impure metals and alloys. If the electron mean free path is considerably less than Co. the coherence length becomes equal to the mean free path, which can easily be less than the penetration depth. Therefore alloys or sufficiently impure metals are usually type-II superconductors [18].

2.14 Lower and Upper Critical Fields

2.14.1. Lower critical field, H_{cl}

We have seen that when a magnetic field is applied to a type-II superconductor it may be energetically favourable for it to go into the mixed state whose configuration has been described in previous sections. However, a certain minimum strength of applied field is required to drive a type-II superconductor into the mixed state. This can be seen by examination of Eq.(2.12), which gives the condition for the free energy to be lowered by the appearance of the mixed state. For a given value of ξ, relative to λ. (in a type-II superconductor, $\xi < \lambda$), we see that H_a must be greater than a certain fraction of H_c . Therefore a certain minimum strength of applied field is required to drive a type-II superconductor into the mixed state, and this is known as the *lower critical field,* H_{c1} . It can be seen that the value *of* H_{c1} relative to H_c decreases as the value of $\kappa (= \lambda / \xi)$ increases. A detailed calculation of the value of H_{c1} for type-II

superconductors with different values of κ is rather complicated. It is found that, very approximately $H_{c1} = H_C / (\kappa\sqrt{2})^{0,65}$ [18].

2.14.2. Upper critical field, H_{c2}

In the previous sections we have shown that if a gradually increasing magnetic field is applied to a type-II superconductor it goes into the mixed state at a "lower critical field" H_{c1} which is less than H_c. Now, in a type-I superconductor, H_c is the field strength at which the magnetic free energy of the superconductor has been raised to such an extent that it becomes energetically favourable for it to go into the normal state. A type-II superconductor in the mixed state has, however, in an applied field, a lower free energy than if it were type-I and perfectly diamagnetic Consequently we may expect that a magnetic field stronger than H_c must be applied to drive a type-II superconductor normal. Fields which *above* H_c the mixed state can have a lower free energy than the completely normal state. The high magnetic field strength up to which the mixed state can persist is called the *upper critical field*, H_{c2}.

At the lower critical field strength H_{c1} a type-II superconductor goes from the completely superconducting state into the mixed state and a lattice of parallel cores is formed. As the strength of the applied magnetic field is increased above H_{c1} the cores pack closer together and, because each core is associated with a fixed amount of flux, the average flux density B in the superconductor increases. At a sufficiently high value of applied magnetic field the cores merge together and the

mean flux density in the material due to the cores and the diamagnetic surface current approaches the flux density $\mu_0 H_a$ of the applied magnetic field (Fig. 2.13). At the upper critical field H_{c2} the flux density becomes equal to $\mu_0 H_a$ and the material goes into the normal state.

We have now seen that, whereas type-I superconductors can exist in one of two states, super-conducting or normal, type-II superconductors can be in one of *three* states, superconducting, mixed or normal [18].

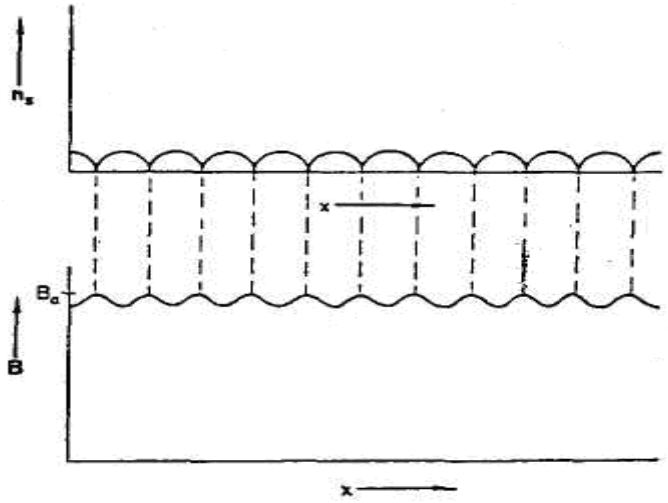

Fig.. 2.13. Mixed state at applied magnetic field srrength just below H_{c2}.

2.15 Applications In Technologies

The discovery of high-temperature superconductors may very well introduce many important technological advances in the future, such as the potential of having superconducting devices in every household. However, many significant material science problems must be overcome before such applications become reality.

Perhaps the most difficult technical problem is how to mold the brittle ceramic materials into useful shapes such as wires and ribbons for large scale applications, and thin films for small devices such as Superconductor Quantum Interferometer Devices (SQUIDs). Another major problem is the relatively low current densities measured in bulk ceramic compounds. Assuming that such problems are overcome, it i_s interesting to speculate on some of the future applications of these newly discovered materials.

An obvious application using the property of zero resistance to dc currents is the exploitation of low-loss electrical power transmission. A significant fraction of electrical power is lost as heat when current is passed through normal conductors such as copper. If power transmission lines could be made superconducting, these dc losses could be eliminated and there would be substantial savings in energy costs.

The new superconductors could have major impact in the field of electronics. Because of its switching properties, the Josephson junction can be used as a computer element. In addition, if one could use superconducting films to interconnect computer chips, chip size could be reduced and speeds would be enhanced because of this smaller size. Thus, information could be transmitted more rapidly and more chips could be contained on a circuit board with far less heat generation.

The phenomenon of magnetic levitation discussed earlier can be exploited in the field of transportation. In fact, a prototype train has already been constructed in Japan which is shown in Figure 2.14. using superconducting magnets on the vehicle (with liquid helium as the coolant). The moving train levitates above a normal conducting metal track through eddy current repulsion. One can envision a future society of vehicles of all sorts gliding above a freeway making use of supercon-

ducting magnets. Some scientists are speculating that the first major market for levitating devices will be in the toy industry.

Another very important application of superconductivity, mentioned earlier, is the construction of superconducting magnets. These high-field magnets are crucial components in the operation of particle accelerators. Currently, all high-energy particle accelerators use liquid-helium-based superconducting technology. Again, there would be significant savings in cooling and operating costs if a liquid-nitrogen-based technology were developed.

An important application of superconducting magnets is a diagnostic tool called magnetic resonance imaging (MRI). This technique has played a prominent role in diagnostic medicine in the last few years because it uses relatively safe rf radiation to produce images of body sections, rather than x-rays. Because the technique relies on intense magnetic fields generated by superconducting magnets, the initial and operating costs of MRI systems are high. A liquid-nitrogen-cooled magnet could reduce such costs significantly. More details concerning MRI are presented in the essay by S. Marshall.

In the field of power generation, various companies and government laboratories have worked for years in developing superconducting motors and generators. In fact, a small-scale superconducting motor using the newly discovered ceramic superconductors has already been constructed at Argonne National Laboratory.

We have already mentioned some small-scale applications of superconductivity, namely SQUIDs and magnetometers which make use of the Joseph-son effect and quantum interference. Such devices are currently being used to measure and interpret the weak magnetic field generated by the brain. Other small-scale applications of

Josephson junctions include their use as voltage standards and as infrared detectors. It should be noted that SQUIDs have been fabricated from films of $YBa2Cu_3O_{7\_},5$, and that Josephson junctions using this compound have been operated at liquid nitrogen temperature and above. It is quite likely that such small-scale applications will be influenced by the new peneration of superconductors in the near future. Unfortunately, because of the brittle nature of these new materials, as well as their low critical current densities, one cannot at this time be optimistic about the future of large-scale applications [20].

Figure 2.14. This prototype train, constructed in Japan, has superconducting magnets built into its base. A powerful magnetic field both levitates the train a few inches above the track, and propels it smoothly at speeds of 300 miles per hour or more. (© T. Matsumoto/SYGMA)

CHAPTER 3

A REVIEW OF HIGH TEMPERATURE SUPERCONDUCTORS

The Bi-Sr-Ca-Cu-O system has layered structure and according to their chemical compositions it three different phases which are called “2201”, “2212”, “2223” [22, 23]. It is generally known that chemical dopping plays very important role in high T_c superconductivity. A large number of elements have been doped into the Bi-2223 system. The objectives of doping studies are to optimize the hole concentration, to introduce pinning centers, to enhance the formation of Bi-2223 phase, and to improve the glass forming ability of the materials [24]. These layered structures are more flexible in composition and more stable in various solvents [25]. Variations in the lattice parameters are observed on doping the system with other elemens at different levels [26-27]. Variations are also observed with the chemical composition conditions [27-28] and the preparation conditions [29-30]. It is useful to observe the variation of both the superconducting properties with changing amounts of different dopants, in order to understand superconductivity better. It was reported that, because of a drastic change in the carrier concentration, the substitution of divalent Ca by trivalent rare-earth elements in the Bi-2212 system

causes a sharp change in transition from a superconductor to an insulator and it also causes a decrease in the lattice parameters *a* and *c* [31,32].

Li, Ti, W and Mo have been doped into BiPbSrCaCuO bulk samples, and it was reported that Li dopping led to an increase in critical current density (J_c), while Ti dopping led to a decrease, and W and Mo dopping didn't contribute a substantial change in J_c [33, 34]. It was observed that substitution of Eu, Dy, and Tm in the Bi–2212 system have caused a transition from superconductor to insulator [34, 35].

It was observed that the partial replacements of Ca by Y, Gd, and Sm in the Bi-2212 and Bi-2223 systems decreased carrier concentration due to structural modulatios and changes in the valency of Cu [32, 36, 37].

D. Rama Sita, R. Signh [38] carried out thermoelectric power (TEP) measurements on the well characterized samples by DC differential technique in vacuum in a closed cycle refrigerator in the temperature range 40-300K. They have carried out the thermoelectric power studies on $Bi_2Sr_2Ca_{1-X}Pr_xCu_2O_y$ $(0 \le x \le 0.6)$ with increase in dopant concentration x, thermoelectric power increases.

R. Singh, D.R. Sita [39] have carried out the thermoelectric power studies on $Bi_2\ Sr_2\ Ca_{1-x}\ Tb_x\ Cu_2\ O_B$ $(0 \le X \le 0.6)$. With increase in dopant concentration x, TEP increases. Samples with $x < 0.4$ are superconducting and the samples with x=0.5 and 0.6 are semiconducting. The TEP for the superconducting samples increases almost linearly with decrease in temperature reaching a maximum value, then decreases sharply around ~ A_C (Critical Temprature).

Z.W.Zhao, S.L. Li, H. H. Wen, X. G. Li [40] have investigated the vortex dynamics in a series of $Bi_2\ Sr_2\ Ca_{1-x}Gd_xCu_2O_{8+\delta}$ single crystals. With increasing Gd

substitution , the plateau of S-T disappears and the collective pinning energy U_c decreases which indicates that the vortex system changes from 3D to 2D and the vortex tends to creep plastically.

Mehmet Ali Aksan, Mehmet Eyüphan Yakıncı [41] have studied on the structural formation, electrical resistance, TEP and thermal conductivity properties on $Bi_2Sr_2 Ca_2Cu_{3-x}Er_xO_{10+\delta}$ (x=0.5 and 1.0) glass-ceramic superconducting system. XRD investigations showed that Er has a large effect on the unit cell parameters of the system. (Both XRD and SEM-EDAX observations indicate a solubility limit for Er ions in the BSCCO system.) They have also found that when Er concentration increased in the Bi-2223 material, crystallization and also melting temperature increases significantly. Electrical resistance measurements showed a decrease on T_c and T_{zero} values of the samples when the Er concentration was increased and its effect on the S is similar for all samples, it suggests that the substitutions of Er changes the distribution of charges between Bi-O and Cu-O planes and more importantly it may be resulted in an increase in the hole concentration in the Cu-O plane.

The electrical resistivity was measured on bar shaped specimens using a standard four probe dc technique in the temperature range between 25K and 130K, with silver paint contacts. And critical current densities of samples were measured at 77K in liquid nitrogen in self-field and at 6mT in the zero field cooled (ZFC) regime by Cabir Terzioğlu et al. [42]. They found that all relevant superconducting properties of the samples decrease when the Sm content is increased in the Bi-2223 system. With increasing Sm concentration the hole carrier concentration decreases both for the Bi-2223 and Bi-2212 phases, and this might cause a suppression in T_c which eventually effects a metal insulator transition. The substitution of Ca^{+2} by the

rare-earth Sm^{+3} provides an additional electron, which in turn, decreases the hole carrier concentration which leads to a decrease of T_c and J_c .

P.E. Kazin et al. [43] have studied on the chemical compatibility of two Ga-containing phases, $(Bi,Sr,Ca)_2Ga_2O_2$ and $Bi_{1.7}Sr_{2.3}Ca_{0.6}Cu_{1.6}Ga_{0.4}O_z$, with Bi-2212 was proved. Ga ions were found to enter in the superconductor phase in the amount of 15–25 mol% and *T* of the superconductor was not suppressed by the Ga substitution. The composite ceramics Bi-2212 + yGa-22 started to melt before 870 ^0C , giving some liquid, Ga-32, Ca_2CuO_3 , and possibly Ga-5 ; at 890 ^0C the system contained only two phases: the liquid enriched with Ga and the solid Ga-32 phase. The melt-processed samples were characterized by the finely structured Bi-2212 / 2201 matrix with big from a few to tens of microns inclusions of the Ga-rich phases. No improvement of flux pinning was observed in the composites. However, the Ga-doping changed the process of Bi-2212 melting, providing more liquid phase along with disappearance of alkaline-earth cuprate and bismuthate phases below 900 ^0C . This can be of use to prepare Bi-2212 whiskers and single crystals.

D. Milliken et al. [44] have studied on the phase formation and thermal treatment optimisation in uranium compound doped $(Bi,Pb)_2Sr_2Ca_2Cu_3Ox$/silver superconducting tapes. A number of U-containing compounds, U_3O_7 , UCa_2O_5 and $UCa_{1.5}Sr_{1..5}O_6$ have been synthesized and used as dopant in Bi-2223 / Ag tapes. The compatibility and interaction between U-compound and Bi-2223 matrix was systematically studied at various thermal processing conditions. Processing parameters at various dopping levels were optimized. $UCa_{1.5}Sr_{1..5}O_6$ shows a remarkable compatibility with Bi-2223 phase, with critical current density reduced by less than 15% at a doing level 1.1 at %, compared with 85% reduction in critical current density at the same doing level for pure U-oxide doping. XRD results show

that $UCa_{1.5}Sr_{1.5}O_6$ had no effect on the Bi-2223 formation while U_3O_7 caused the degradation of Bi-2223 phase up to 50% at the doping level of 1.1 at %. U-compound dopping also widens the processing window to $15\,^0C$.

A. Marifio et al. [45] carried out the resistivity and thermoelectric measurements by using the four probe d.c. method and the differential technique with a temperature gradient, $\Delta T \approx 0.3$ K across the sample respectively. The other parameters fluctuations (OPF) effects on the S (T) are driven mainly by $\sigma(T)$ because L (T) is nearly reduced temperature independent, i.e. , the inhomogeneities generated by the silver addition do not affect substantially the behavior of L (ε) in all MFR. For Iow-Ag doped level $(0 \le x \le 0.005)$ BSCCO (2223 and 2234) samples the behavior with reduced temperature of S (ε) and $\sigma(\varepsilon)$ is similar for all samples and independent of Ag-addition. S(T) is less sensitive than ρ(T) to the inhomogeneities produced by Ag-dopping.

Z.Y. Jia et al. [46] have studied on Effects of nano-ZrO particles on the superconductivity of Pb-doped BSCCO. The *T* onset and the transition width of samples c with *x* less than 20 mol%, as determined by standard dc four-terminal method, are about 110 and 3 K, respectively. The X-ray diffraction (XRD) patterns of ZrO -doped samples with various contents 2 show that most of the peaks belong to Bi-2223 phase with a few of low intensity belonging to Bi-2212 and other unknown nonsuperconducting phases. Differential thermal analysis (DTA) is used to investigate whether the impurity phases were created by the reaction between ZrO_2 and Bi-2223. There is no evident heating-effect peak in DTA curves. They have also measured the temperature dependence of AC susceptibility of samples. In summary, experimental results show that the artificially introduced nano-ZrO_2 particles have not remarkable effects on the critical transition temperature of Pb-doped Bi-2223.

DTA measurement cannot exclude the possibility of reactions between doped ZrO_2 and Bi-2223. However, from the magnetic hysteresis loops' measurements and the critical current density calculation based on the Bean model, the doped nanometer-sized ZrO_2 with proper contents is proved effective flux pinning center in the Bi-2223 matrix. Thus, the route of artificially introducing nanometer-sized oxide particles as strong flux pinning centers in the processing of large bulk BSCCO or further PIT-textured Ag / BSCCO thick tapes is a promising technique for industrial-scale application.

A. Sanchez et al. [47] report measurements of resistivity, Nernst and Seebeck efects of $(Bi_{0.8}Pb_{0.2})_2\ Sr_2\ Ca_3\ (Cu_{1-x}\ Ag_x\ )_4\ O_{12+\delta}$ bulk samples with $0 \le x \le 0.02$. The temperature and the magnetic field dependence of these quantities were measured in the mixed state at low-magnetic fields between 0 and 1.2 T. The behavior of $\rho(T)$ as a function of magnetic field and for different Ag concentrations at $T \le T_c$ ($T_c \sim 106K$) correlates well with the S(T) behavior. In the presence of the applied magnetic field the usual broadening of the temperature dependence of both coeffcients is observed. The broadening of the resistive transition, however decreases by increasing Ag-content, which can be due to the increasing of the flux-pinning centers. The normalized Nernst electric field, close below T_c, increases by reducing temperature, goes through a maximum and becomes very small at the same temperature as the resistivity, because of the increasing flux-pinning strength. The maximum shifts to lower temperature by increasing the magnetic field. A decreasing of the Nernst electric field by increasing the Ag-content it was observed, because of a reduction of the vortex velocity. This behavior and the observed decreasing of the width of the resistivity transition at zero-magnetic field, as a function of Ag-content, can be associated to the formation of pinning centers by Ag addition. The transport

entropy (S) derived from Nerst electric field and ρ steeply increased with decreasing temperature at $T \leq T_c$.

Mustafa Tepe et al. [48] have studied of doping vanadium with $(Bi,Pb)_2Sr_2Ca_2(Cu_{1-x}V_x)_3O_y$ at low concentration of x= 0.01–0.03. The superconductivity of the samples were determined by employing a.c. resistivity, a.c. susceptibility and XRD measurements. For the low concentration range of vanadium they have observed some enhancement effects in stabilizing the high T_c phase, resulting in increase in the volume fraction of it. The magnitude of the resistance in the normal state decreases for the samples with x = 0.00–0.02, but it begins to increase again for x = 0.03. The onset temperature, T_c^{onset}, values for these samples were all measured about 110 K. The zero resistance temperature, T_{co}, for the samples with x = 0.00 up to x = 0.02 increases from T_{co} =102.7K to T_{co} = 103.9 K and it decreases again to 101.1 K for x = 0.03. Lowering of T_c and J_c for further increase in vanadium shows that V starts entering the lattice, replaces Cu in the CuO2 planes and that lowers T_c^{onset} due to intragrain and *Tc* of the intergrain regions. It is reported that dopping the single-phase $Bi_2Sr_2Ca_1Cu_2O_8$ by vanadium in the range of x=0.01 to 0.05 lowers T_c seriously and this causes a linear decrease in the *c*-lattice parameter with increasing V content. The observed enhancement in their results might find an explanation in regarding the roles of two dopants, namely Pb and V simultaneously. They think that Pb partially replaces Bi and stabilizes the high-T_c phase. But at low concentrations (for x=0.0 to 0.02) the V^{+5} cations did not enter the crystal structure and by lowering the melting point has helped to increase the 2223 phase, parallel to Pb. The significant decrease in *Tc* for the x=0.03 value indicates the substitution of vanadium into the CuO2-planes, hence modifying the hole concentration (by replacing Cu atoms with V within the plane), where

superconductivity occurs. The enhancement in J_c also for the same vanadium range shows that the pinning strength is increased by dopping with vanadium at low concentrations.

Vilas Shelke et al. [49] have investigated the effect of Hg addition on the superconducting properties of BiSrCaCuO system. Polycrystalline samples with nominal composition $Bi_2Sr_{2-X}Hg_XCa_2Cu_2O_Y$ and $Bi_2Sr_{2-X}Hg_XCa_2Cu_3O_Y$ were synthesized and used to investigate the phase evolution by XRD, superconducting behaviour by *R–T* measurement and the structural grain boundary effects by SEM. Addition of Hg decreases the melting temperature of composition to 820^0C , but it is not having any influence on the chemical reaction kinematics so as to favour the growth of the 2223 phase. A considerable increase is observed in the *T* values of both the samples after additional annealing. Unlike Hg-based superconductors, they have synthesized Hg-added BiSrCaCuO samples in open atmosphere. With both types of starting compositions 2212 and 2223, the finally obtained phase was Bi-2212. Neither any mercury-related phase was formed nor mercury was incorporated in the system. Thus, the role of Hg was like a catalyst. Although the maximum *T* obtained in this case 92 K is zero within the range of that obtained by proper tuning of hole concentration, the remarkable feature is the possibility of further *T* enhancement by Hg addition. At the same time, they have observed *T* depression with 2212-type starting composition. Such a variation of *T* has been attributed to the tuning of optimal charge carrier concentration. Also, an improved grain diffusion has been observed in our highest *T* samples.

N.D. Zhigadlo et al. [50] investigated the influence of Cs doping and heat treatments on the phase formation, microstructure development and normal, superconducting state properties of (Bi,Pb)–Sr–Ca–Cu–O superconductors. Samples

with nominal composition $Bi_{1.7}Pb_{0.3}Sr_2Ca_2Cu_3Cs_xO_y$, x=0.0 – 1.0, were prepared and characterized by X-ray diffraction, scanning electron microscopy, electron probe microanalysis, resistivity, low field magnetic susceptibility and critical current density measurements. All samples mainly consist of 2212 and 2223 phases, with the 2223 phase being dominant. However, the amount of 2223 phase depends on the Cs content. Samples with x=0.0 and 0.1 contain 76% and 82% of the 2223 phase, respectively. With increasing x the intensities of the peaks of the 2212 phase decreased and for samples with x=0.3, 0.6 and 0.7 the amount of the 2223 phase was 88%, 85% and 83%, respectively. With further increase of x, the percent ratio of the 2223 phase decreased and for samples with x=1.0, the amount of the 2223 phase was 72%. Addition of Cs to $Bi_{1.7}Pb_{0.3}Sr_2Ca_2Cu_3O_y$ was found to decrease the normal state resistivity and increase J_c. With the increase of Cs dopping the intensities of the peaks of the 2212 phase decreased and for samples with x=0.4–0.8, an almost single (~ 93%) high-T_c 2223 phase was detected. This indicates that the volume fraction of the 110 K phase increases with Cs dopping. With further increase of Cs (x=0.9, 1.0) the peaks of the 2212 phase increased. No systematic changes in the lattice parameters of 2223 phase were found. However, the volume of the unit cell significantly increases in all cases in comparison to undoped samples. In spite of the fact that X-ray data show significant volume of 2212 phase for samples with x=0.0, all samples show only one superconducting transition with $T_{c,\,zero}$ = (102.6 –106.0 K) and $T_{c,\,onset} \approx$ 112 K, caused by the 2223 phase. It is seen that heat treatment of samples in regime-C decreases the normal state resistivity, increases the critical current density and leaves T unchanged. The magnetic properties of samples where Cs was added were better than for the samples with

x=0.0, indicating that the magnetic properties of the samples are enhanced by the addition of Cs.

Sandeep Singh et al. [51] studied $Bi_2Sr_2\ Ca_{1-x}\ Sm_x\ Cu_2\ O_{8+\delta}$ and $Bi_2Sr_2\ Ca_{1-x}\ Sm_x\ Cu_{1.95}\ Co_{0.05}O_{8+\delta}$ systems through X-ray and electrical resistivity measurements. The DC resistivity of rectangular bar shaped samples was measured in an APD closed cycle helium refrigarator using four probe technique. AC suseptibility measurements were performed at 0.1 Oe and at 73 Hz using phase sensitive detection technique. The back ground intensity remains nearly unchanged in Sm samples whereas it shows slight increase in Sm, Co samples. They noticed that for low Sm concentration ($x < 0.3$) the most intense line observed from the (115) plane in both types of samples. However, with increase of Sm concentration the (117) plane gives rise to the peak of highest intensity. The present samples exhibit an increase in a-lattice parameter and a decrease in c-lattice parameter wih increasing x. The decrease in c-lattice parameter in Gd and Sm doped samples, however, is not roportional to the ionic radii difference of the ions. This is due to the fact that a larger concentration would be opposed by the repulsive forces between cationic layers. Surprisingly, SmCo samples do not show an increase of T_c though the samples were prepared in the same way as the Sm samples. This can occur if the excess holes in this system get localized in the vicinity of impurity Co^{+2} ions in the CuO_2 plane. It is evident that superconductivity vanishes for $0.5<x<0.6$ in the Sm samples, whereas in the SmCo samples it vanishes for $0.3<x<0.4$. The vanishing of the superconductivity for values of the x between 0.5 and 0.6 in the Sm samples is identical to the Gd doped 2:2:1:2 system. With increasing Sm concentration no rapid decrease in T_c is observed. Also the trend of decrease of T_c beyond x = 0.20 in SmCo sample is identical to that of Sm samples. This shows a negligible interplanar

magnetic interaction in SmCo samples and suppression of T_c in both systems is due to identical reasons. Sm concentration affects transition width, increases normal state resistivity and residual resistivity. ρ_0 values of the SmCo samples are higher than in the Sm samples. (SmCo samples have higher amount of disorder than the Sm samples.) When the Sm concentration increased, impurity scattering in the CuO_2 plane increases. The samples which are in the insulating state follow 3D variable range hopping of conduction mechanism with energy dependent density of states.

In this work we have investigated the effect of the partial substitutions of Ca by Sm in the Bi-2223 superconducting samples which are prepared by standard solid-state reaction methods, the physical and microstructure properties of the BSCCO by performing DC resistivity, critical current, XRD measurements, and to compare the outputs with other experimental results.

CHAPTER 4

CRYSTAL STRUCTURE

4.1 Introduction

Compounds with the perovskite structure have the formula of ABO_3. A is a relatively large ion in the center of cube (unit cell), and B is a smaller ion at the corners, while oxygen ions are at the unit cell edges. The perovskite structure is also described with the A ion at the corners of a cubic unit cell, the B ion in the center, oxygen ions in the faces. For touching ions, it can be seen from geometric considerations that the $\sqrt{2}$ times the B-O distance along the edge of the cube is equal to the A-O distance [52].

Such an atomic arrangement was seen in compound of $CaTiO_3$ as shown in Figure 4.1. Ti^{+4} is a relatively ion in the center of unit cell, and Ca^{+2} is a smaller ion at the corners, while oxygen ions are at the unit cell edges [53].

As an additional requirement, to keep the electrostatic balance, the sum of the charges on the A and B ions must add up to +6. Thus, A+B charge combinations of 1+5 ($KNbO_3$), 2+4 ($BaTiO_4$) and 3+3 ($LaAlO_3$) are possible while there are some compounds with the cubic perovskite structure, most of the compounds actually have structures distorted from cubic symmetry except at elevated temperature [54].

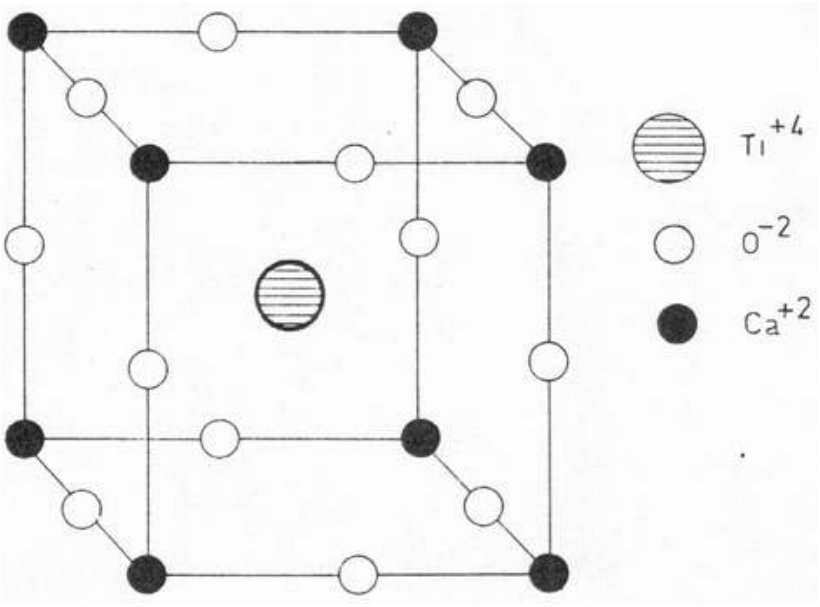

Figure 4.1: Perovkite structure of $CaTiO_3$

The perovskite compounds of greatest interest are those which exhibit variations from the ideal cubic stoichiometric ABO_3 phases. It is possible to have vacancies in the A position (such as the tungsten bronzes as in Na_xWO_3), oxygen deficiencies (such as in $SrVO_{2.5}$), and unusual oxidation states (such as Ti +3 in $LaTiO_3$).

4.2 Crystal Structure of the Bi-based systems

The three phases of the Bi-based system have similar crystal structures as shown in Fig. 4.2. The crystal lattice parameters a and b are mostly reported to be equal to each other and about 5.4 $\overset{0}{A}$; in some references they are not equal but the difference is very small. Both parameters are the same for all three phases. Some

other references, on the contrary, report that lattice parameters *a* and *b* are around $3.8\,\overset{0}{A}$. This is because they quote the crystallographic structure as body centred instead of face centred. Each superconducting phase of the Bi-based system has a different c axis lattice parameter. The 2201 phase has a c-axis of ~$24.4\,\overset{0}{A}$, 2212 phase has a c-axis of ~$30.7\,\overset{0}{A}$ and 2223 phase a c-axis of ~$37.1\,\overset{0}{A}$ [24].

It is well known that the 2201 phase is formed first and is transferred into 2212 phase via solid-state reactions. The 2223 phase is formed finally from 2212. For instance, Danusantoso and Chaki report that the 2201 phase crystallizes from amorphous precursors at the beginning of annealing and is then transformed into the superconducting 2212 phase through the diffusion of calcium. A liquid phase in partially melted samples offers fast diffusion paths for the elements required to form the 2223 phase. The formation of the 2223 phase starts from the 2212 compound by a liquid phase reaction and is strongly influenced by the presence of Ag. Silver participates in the reaction of the oxides and enables the system to form a partial melt around 830°C. It has also been suggested that Sr and Bi can replace Ca and Pb respectively in the impurity phase Ca_2Pb0_4, eventually leading to the easier formation of the 2223 phase. A Pb enriched liquid phase enhances dissolution of the

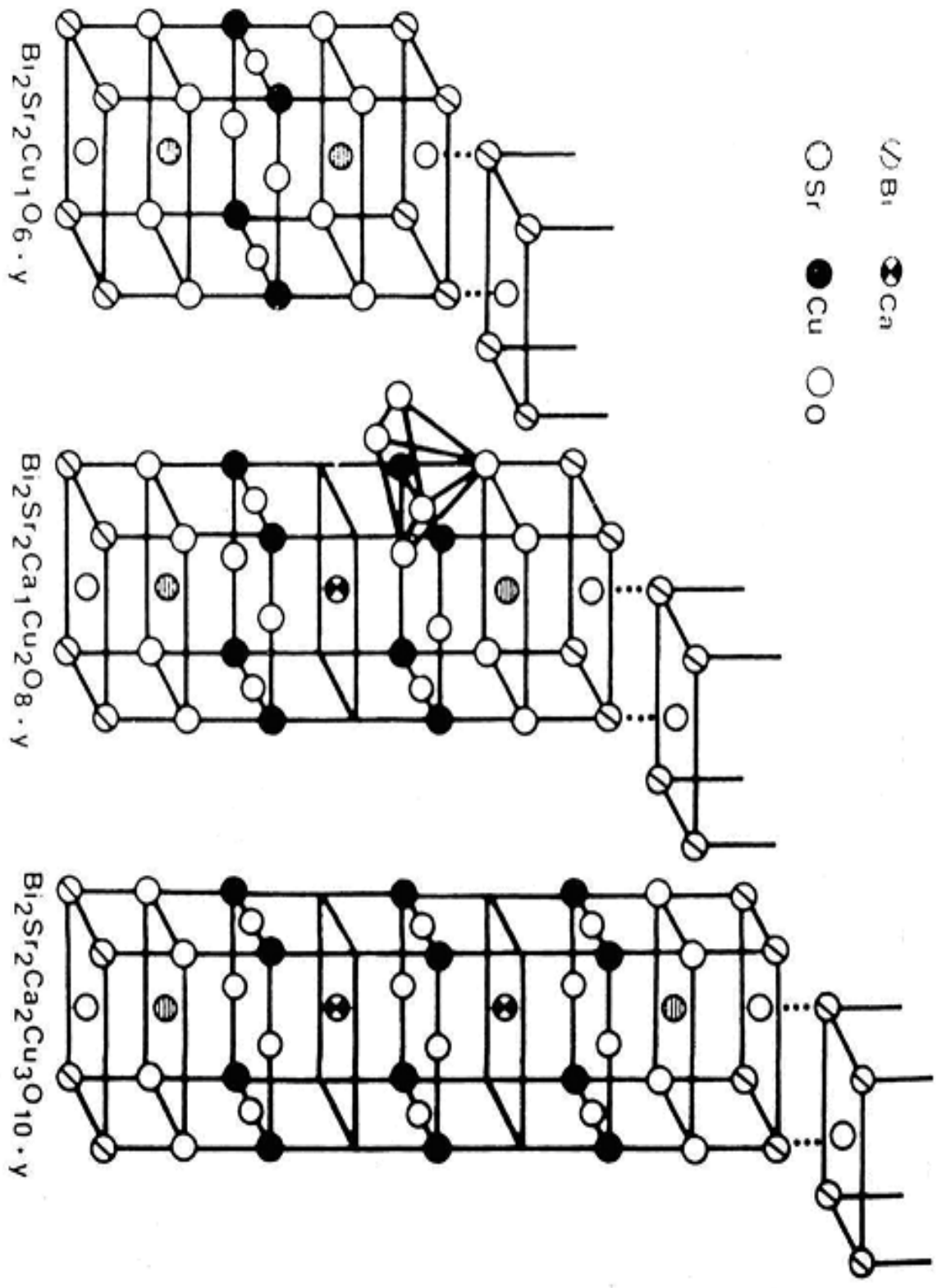

Figure 4.2. Crystal substructures of the phases of the phases of the Bi-based system. The phases are 2201, 2212, 2223 and their c axis lengths are (in angstrom) 24.6, 30.7, 37.1, respectively.

2212 phase and impurity phases, especially of the high temperature melting compounds [24].

The crystal structure and the space group of 2212 and 2223 phases are subjects of conflicting reports. This is probably because of minor differences in the crystal lattice of the material due to the particular fabrication process as well as the local properties of the part of the sample examined. For example, X-ray precession photographs show systematic changes due to the slight differences of the cell parameters between a number of single crystals. Distortions of the crystal structure due to the elements of the system substituting for each other may also happen under different preparation conditions, eventually leading to slight changes in the crystal structure. As an example, Sastry et al. have reported that Ca sites are disordered with-likely substitution of Bi/Sr, and Sr sites are disordered by partial substitution of Bi. The structure of their material as pseudotetragonal and emphasize the ease of intergrowths, stacking alternatives, and stacking faults due to small free energy differences between phases, which differ only in the numbers of CaCuO slabs. The 2212 phase can intergrow in the 2223 phase matrix. Powder XRD, single crystal XRD, convergent beam electron diffraction, HREM (high resolution electron microscopy), NMR (nuclear magnetic resonance) and neutron diffraction methods are used for structural studies. The 2223 and 2212 phases have a face-centred orthorhombic structure according to some authors [24]. Some other reports mention the crystal structure as pseudotetragonal face, centered or pseudotetragonal body centred. 14/mrom, I4mm, Fmmm, Pcnn, Pmnn, Amaa are suggested as the space group of these materials. High quality single crystals of undoped 2223 phase are necessary before the last words on the space group of the 2223 phase can be given. Sihan et al. [55] have suggested that the anomalous change of ultrasonic velocity,

which they observed near 200 K in a 2212 BSCCO sample, indicates another possible structural change or a phase transition.

CHAPTER 5

EXPERIMENTAL PROCEDURE

5.1 Preparation of Superconducting $Bi_{1,6}Pb_{0,4}Sr_2Ca_{2-x}Sm_xCu_3O_y$

Samples of nominal compositions $Bi_{1,6}Pb_{0,4}Sr_2Ca_{2-x}Sm_xCu_3O_y$ (x= 0.0, 0.0005, 0.001, 0.005, 0.01, 0.1, 0.5, 1.0, and 1,5) were prepared by standard solid-state reaction methods. The starting materials (Bi_2O_3, PbO, $SrCO_3$, CaO, Sm_2O_3 and CuO), taken in stoichiometric proportions, were ground and calcined at various temperatures between 800^0C and 850^0C for 24 h. The powder was well mixed, pressed into pellets 13mm in diameter and sintered at various temperatures between 860^0C and 950^0C for 200 h, during which time intermediate grindings were performed to complete the solid-state reaction. The heating and cooling rates of tube furnace were chosen to be 5^0C / min and 3^0C / min, respectively. After cooling to room temperature, the pellets were cut into rectangular bars (2.9mm x 2.1mm x 12.1mm) for resistivity and critical current measurements. All samples were prepared by Mustafa YILMAZLAR in Kırıkkale University.

5.2 X-Ray Diffraction Analysis

Phase purity and lattice parameters were determined by XRD. XRD data were taken using a Rigaku D/Max-IIIC difractometer with CuKα radiation in the range $2\theta = 4 - 60^0$ with a scan speed of 3^0/min and a step increment of 0.02^0. The accuracy in determining the lattice parameters was $\pm 0.001 \overset{0}{A}$. These measurements were made by Mustafa YILMAZLAR at KKU.

Figure 5.1: The whole system. (Magnet, Cryostat, Power supply, Multimeter, Computer)

5.3 Measurements

Zero resistance transition temperature (T_c) and critical current density (J_c) were used to characterize superconducting properties of the samples. The electrical resistivity was measured on bar-shaped specimens using the standard four-probe dc technique, in the temperature range between 25 K and 130 K, with silver paint contacts as shown in

Figure 5.2. The transition temperature was taken to be the zero resistivity temperature. In the resistivity measurements (R-T), a very low current is driven through the sample, called "test current". The measured zero resistivity, critical temperature, T_c^{offset}, is the temperature at which the supercurrent carrying capacity of the sample is equal to the test current applied. R-T curves are usually between room temperature and T_c^{onset}. T_c^{onset} is the temperature at which R-T curve deviates from linear behavior. Critical current densities of samples were measured at 77K in liquid nitrogen. The critical current density, $J_{c,}$ was determined from the current-voltage characteristics. The critical current, $I_{c,}$ was determined at the onset of a voltage with a criterion of $2\mu V/cm.$. Magnetoresistivity measurements were performed by using four-probe method with dc current of 10mA between 25-130 K temperature interval under constant magnetic field 0, 0.3, 0.6 Tesla respectively. Magnetic field as a function of resistance measurements were performed by using four-probe method with dc current of 10mA under changing magnetic field between 0 to 0.6 Tesla (H vs. R) at constant temperature.

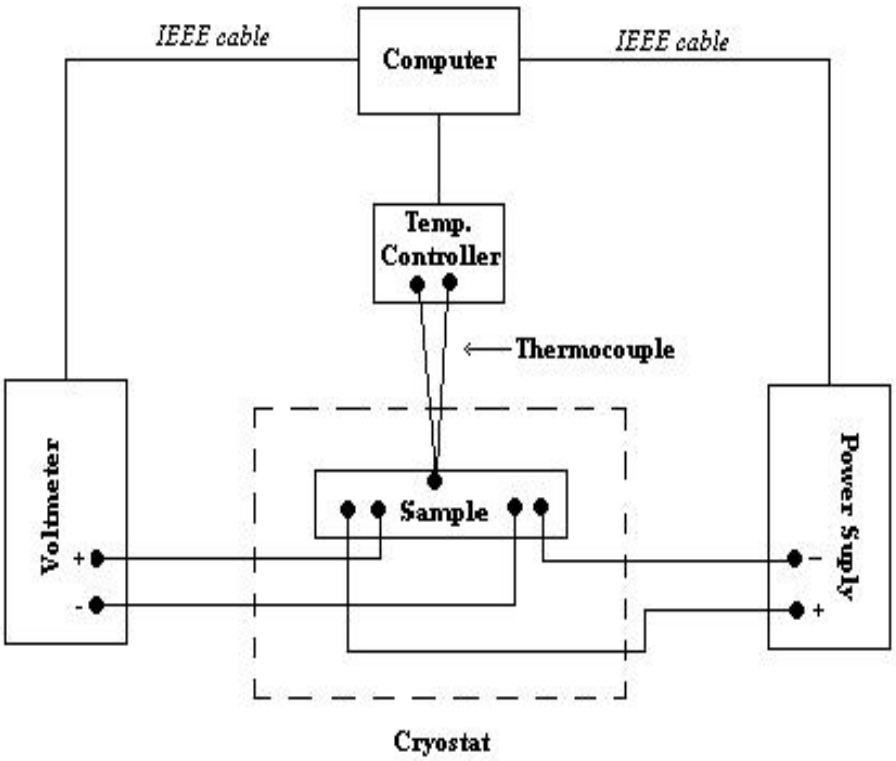

Figure 5.2: Schematic diagram of the four-probe method.

CHAPTER 6

RESULTS & DISCUSSION

6.1. X Ray Diffraction Analysis Results

The XRD patterns of samples with x = 0, 0.01, 0.1 and 1.5 recorded at room temperature are shown in Figure 6.1.1 Miller indices are indicated in the figure. It is observed that the intensities of the peaks corresponding to the high-T_c (Bi-2223) phase decrease and intensities of the peaks corresponding to low- T_c (Bi-2212) phase increase with the increasing substitution of Sm for Ca. When the Sm content was $x \geq 0.1$, the Bi-2223 phase reflections were completely absent and only those belonging to the Bi-2212 phase were present (Figure 6.1.1). A few small peaks were not identifiable.

The relative volume fractions of the Bi-2223 and Bi-2212 phases were determined from the peak intensities of the same particular reflections, using the following well-known expressions [42].

$$f_{(2223)} = \frac{\Sigma I_{H(hkl)}}{\Sigma I_{H(hkl)} + \Sigma I_{L(hkl)}} \quad (1)$$

$$f_{(2212)} = \frac{\Sigma I_{L(hkl)}}{\Sigma I_{H(hkl)} + \Sigma I_{L(hkl)}} \quad (2)$$

Here $I_{H(hkl)}$ and $I_{L(hkl)}$ are the intensities of the (hkl) diffraction lines for the Bi-2223 and Bi-2212 phases, respectively which is shown in Figure 6.1.1. With increasing Sm concentration up to x=0.01, the volume fraction of Bi-2223 phase decrased and that of Bi-2212 phase increased; whereas for samples with x≥0.1, the Bi-2223 phase was totally absent. The lattice parameters for the two phases were determined by using a non-linear least square method. Both the d-spacings and the weak intensity ratios of these two phases were in good agrement with previous publication [56-57].

The variation of the lattice parameters a and c as a function of the amount of Sm in the samples is shown in figure 6.1.2 It is observed that parameter a increases slightly and parameter c decreases significantly with increasing Sm content as listed in table 6.1.1 . A smilar phase transformation has been reported by Zendbergen et al. [58]. The behaviour of the lattive parameters can be explained by the increase of the oxygen content in the unit cell by the replacement of Ca^{2+} and Sm^{3+} in the structure. It was speculated that the excess of the oxygen goes into the bismuth oxide layers causing an increase in parameter a and consequently a decrease in parameter *c*. It is also believed that the increase of parameter *a* and the decrease of parameter *c* is due to the incorporation of Sm ions into the intersitial sites in the unit cell rather than occupation of the Ca sites.

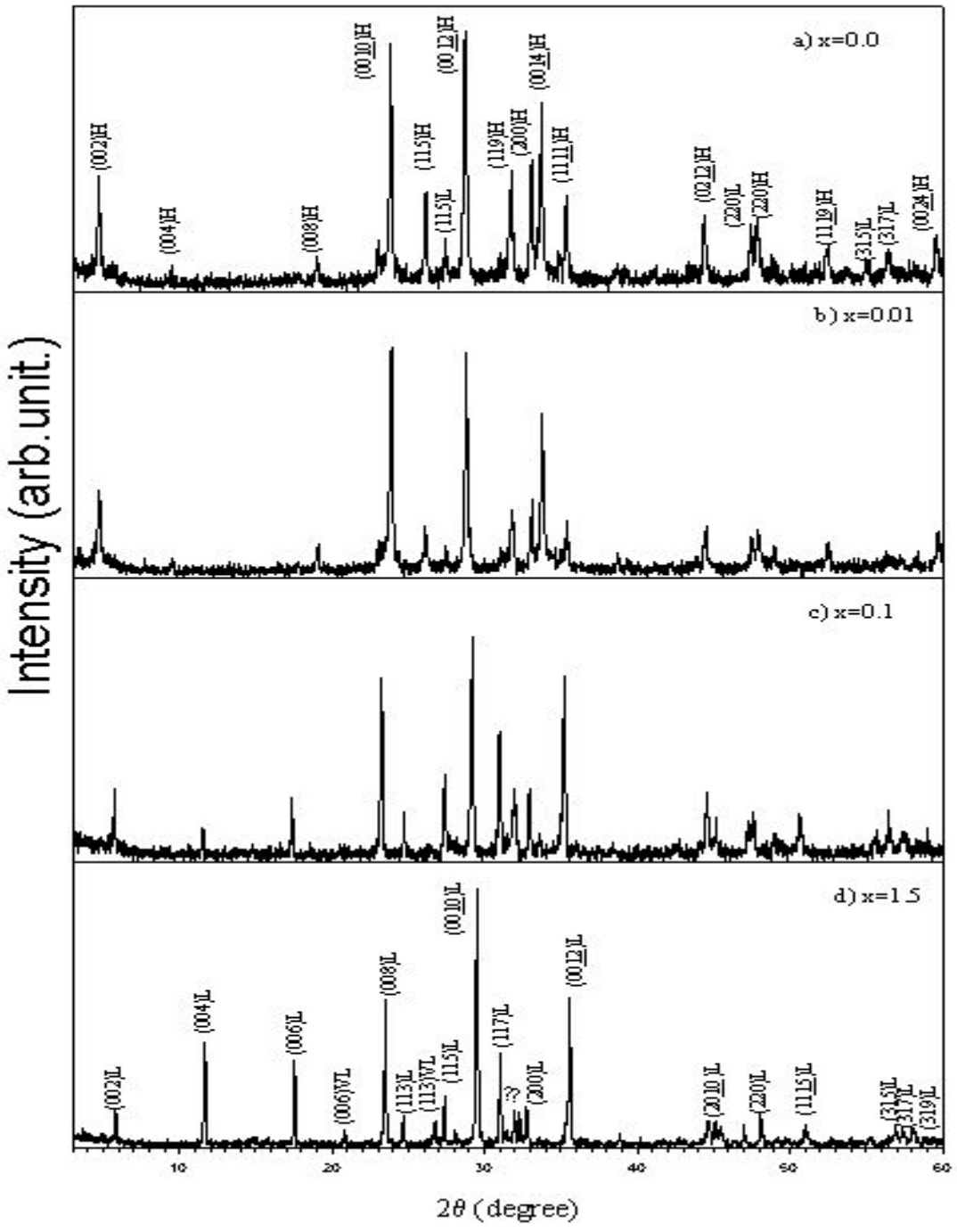

Figure 6.1.1: The XRD patterns of samples with x = 0, 0.01, 0.1 and 1.5 recorded at room temperature.

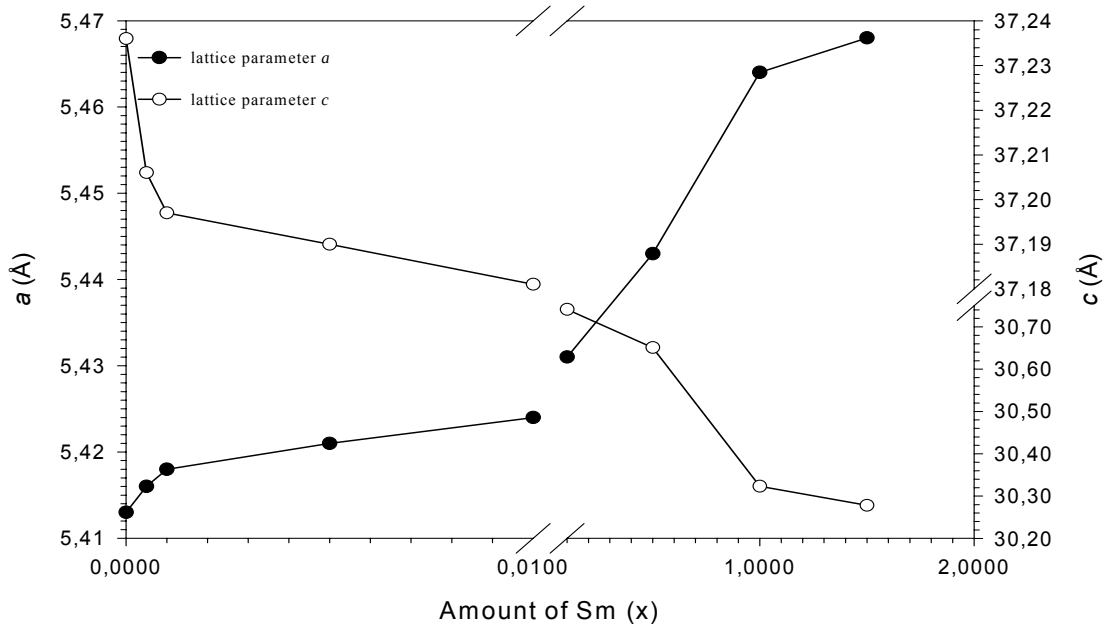

Figure 6.1.2: The variation of the lattice parameters a and c as a function of the amount of Sm in the samples.

Table 6.1.1: Lattice parameters of the samples related with Sm concentration.

Sm Content (x)	Lattice parameters (Å)		Cell Volume (V) ($Å^3$)	Volume fraction (%)	
	a	*c*		Bi-2223	Bi-2212 + unknown phases
0	5.413	37.236	1091.036	94	06
0.0005	5.416	37.206	1091.366	92	08
0.001	5.418	37.197	1091.908	83	17
0.005	5.421	37.190	1092.291	79	21
0.01	5.424	37.181	1093.857	74	26
0.1	5.431	30.741	906.729	---	100
0.5	5.443	30.651	908.074	---	100
1.0	5.464	30.323	905.302	---	100
1.5	5.468	30.278	905.283	---	100

6.2. Electrical Resistivity Results

The electrical resistivity as a function of temperature was measured for the x=0.000, 0.0005, 0.001, 0.005, 0.01, and 0.1 Sm samples as shown in Fig. 6.2.1, respectively. As can be seen from the figure, the transition temperature decreases with increasing Sm concentration which is in good agreement with the literature for different substances doped (Cu, Gd, Er, Sm) [42, 59, 60, 24, 25]. For the sample without Sm, the T_c^{onset} and T_c^{offset} of the superconducting transition were determined to be 116 K and 107 K. It is seen from Fig. 6.2.1 that, with increasing concentration of Sm, T_c^{offset} ranges from 107 K to 45 K, which is consistent with the literature [42] .

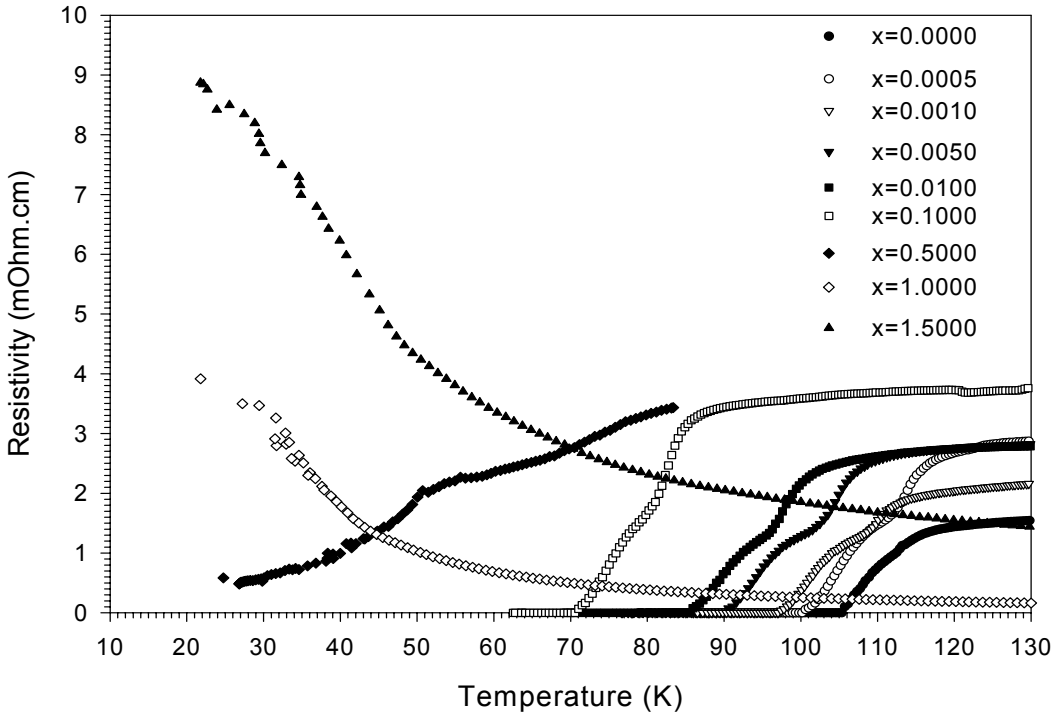

Figure 6.2.1: The electrical resistivity as a function of temperature.

The rate of decrease in resistivity increases with decreasing Sm concentration as can be seen in literature for different substances dopped (Cu, Gd, Er, Sm) [42, 59, 60, 24, 25]. The transition curves indicate two-step (double step) transitions, which is an indication of two phases present in the sample and it is related to a structural phase transformation. We believe that the double step resistive transition is an indication of weak links in the sample, while the onset transition temperature is an intra-grain property. We have also observed that the transition width ΔT (T_c^{onset} - T_c^{offset}) increases with increasing Sm concentration [42]. In the normal state, all samples show a linear temperature dependence of the electrical resistivity $\rho = \rho(0) + aT$. Residual resistivity increases while critical transition temperature decreases with increasing x from zero to 0.1 Sm as can be seen in literature same results were obtained for different substances doped (Cu, Gd, Er, Sm) [42, 59, 60, 24, 25]. These results suggest that Sm atoms substitute Ca atoms.

6.3. Magnetoresistivty Results

The electrical resistivity as a function of temperature was measured in an external magnetic field up to 0.7 T for the x= 0.0005, 0.001 Sm samples as shown in Fig. 6.3.1,6.3.2 respectively. It is seen from Fig. 6.3.1-2 that, with increasing applied magnetic field, T_c^{offset} ranges from 89 to 60 for x=0.0005 Sm, 85 to 54 for r x=0.001 Sm, 79 to 45. It is observed that the broadening of the resistivity transition width increases with increasing external dc magnetic field for all samples [59]. The width of intragrain transition ΔT_c increases with increasing the magnetic field from zero to 0.7 T.

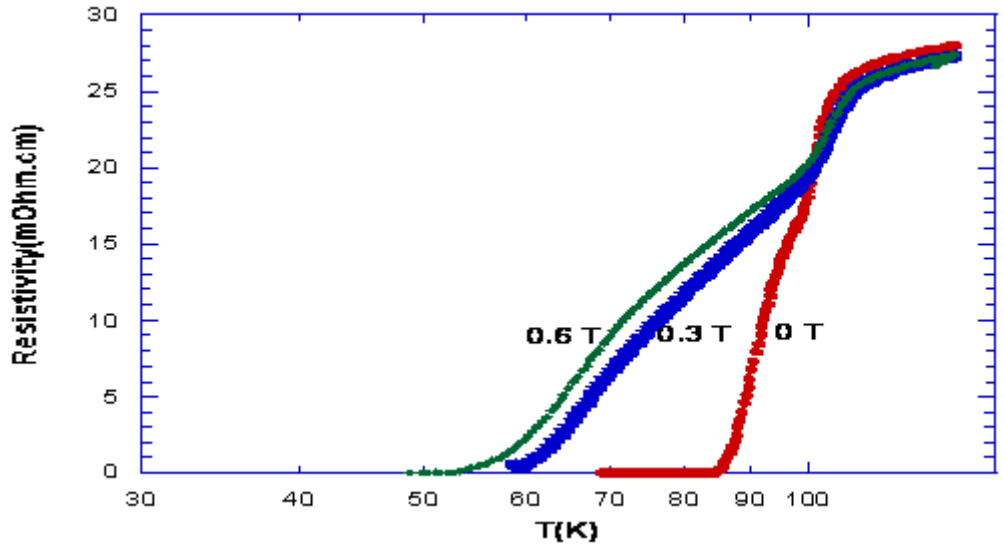

Figure 6.3.1: Temperature dependence of resistivity with changing applied magnetic field for $Bi_{1.6}Pb_{0.4}Sr_2Ca_{2-x}Sm_xCu_3O_y$ (x= 0.0005) samples.

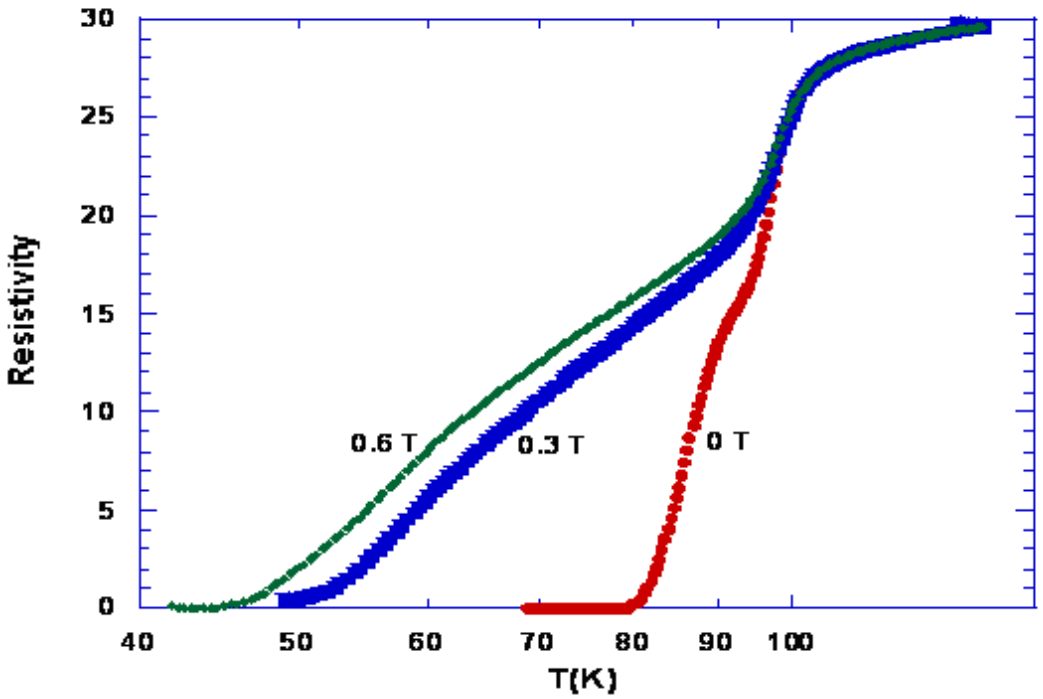

Figure 6.3.2: Temperature dependence of resistivity with changing applied magnetic field for $Bi_{1.6}Pb_{0.4}Sr_2Ca_{2-x}Sm_xCu_3O_y$ (x=0.001) samples.

Below T_c, the thermally assisted flux flow (TAFF) is an important dissipation mechanism inducting a long resistance tail. TAFF theory predicts that in the low current limit the resistivity obeys the relation of Eq. (6.3.1). By rewriting Eq. (6.3.1) in the form

$$\ln(\frac{\rho}{\rho_0}) = -\frac{U_0}{k_B T} \quad (6.3.1)$$

we obtain that U_0 is the slope of the Arrhenius plot for $\ln(\rho/\rho_0)$ versus 1/T. Fig. 6.3.3 shows magnoteresistivity data in an Arrhenius representation for x=0.0005 Sm sample. As mentioned before, we use linear fits to the apparently linear parts of the curves (in the low resistivity parts) to extract activation energies, U_0, from the graph. From the slope lines we get activation energies as a function of external magnetic field as shown in Fig. 6.3.4 (see Table 6.3.1). In literature a lot of workers used this technique to evaluate the activation energies [61, 62, 63, 59, 64, 65]. It can be seen from the graph, the activation energy decreases significantly with increasing magnetic field up to 0.6 T for all samples which is consistent with previous work [64]. It is also observed that the activation energy decreases with increasing Sm content.

Table 6.3.1: Activation Energy Values of BISSCO

Sm content	Activation Energy at 0 T (K)	Activation Energy at 0.3 T (K)	Activation Energy at 0.6 T (K)
0.1	569.83	348.01	285.85
0.01	6373	3656	3504
0.005	7239	1902	1696
0.001	7733	1513	851.8
0.0005	10069	1420.7	1311.9

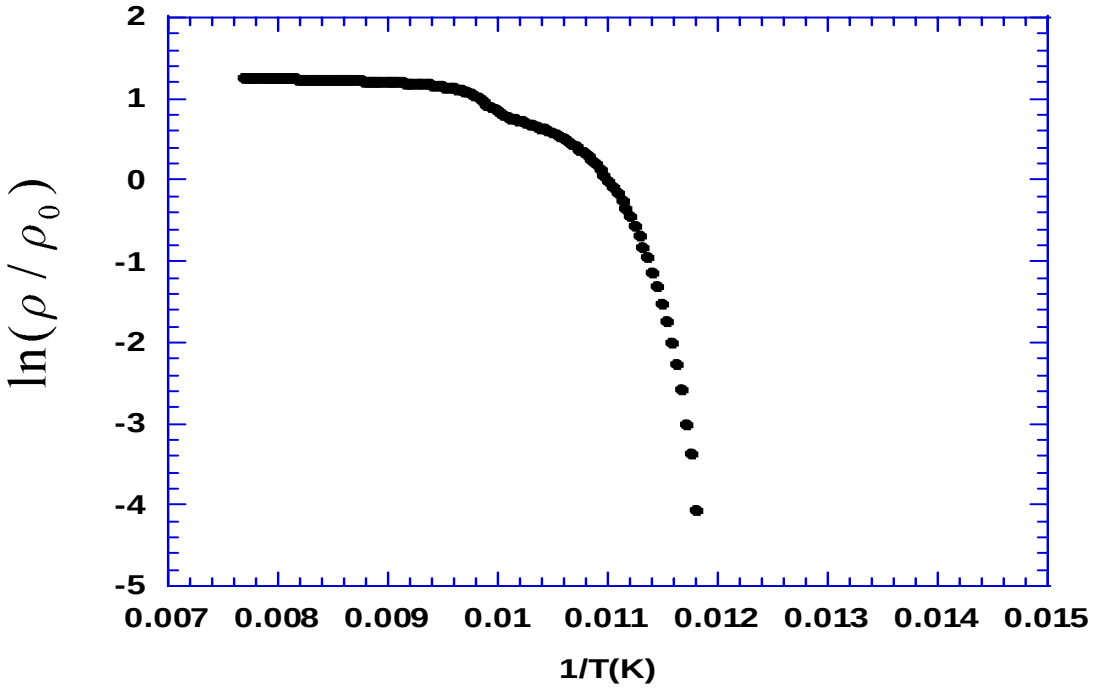

Figure 6.3.3: $\ln(\rho / \rho_0)$ versus 1/T shows magnoteresistivity (Arhenius plot).

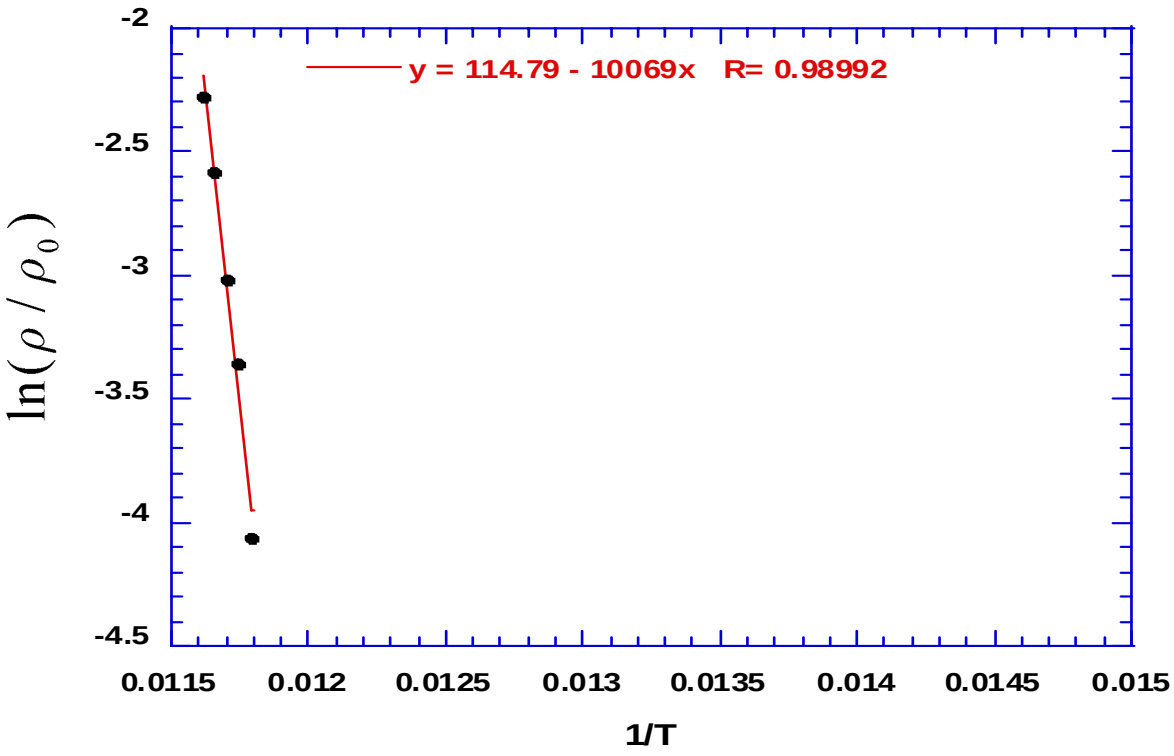

Figure 6.3.4: $\ln(\rho / \rho_0)$ versus 1 / T (1 / Kelvin) for 0.0005 Sm doped sample. The slope of this graph gives activation energy.

Next, we want to investigate the temperature dependence of peak field H_p, deduced from the measurements of the electrical resistivity for both samples. Fig. 6.3.5 shows the corresponding data of zero resistance temperature at various selected magnetic fields. These temperatures are comparable to irreversibility or depinning temperatures. It is well to depin the flux line since lowering the temperature increases the pinning force. This results in a shift of the zero resistivity or the irreversibility temperature downwards as the magnetic field increases [61]. It is observed that the

irreversible region of H_{irr} versus T graph extends to higher temperatures for all samples. For the irreversibility, a representation:

$$H_{irr} = H_0(1-T/T_c)^n \,, \qquad (6.3.2)$$

near T_c has been established. Both pre-factor H_0 and n are model-dependent parameters [61]. As can be seen from Fig. 6.3.5, the power low relation give a good fit to experimental data for all samples and we found the value of n is 3.22 and this is in good agreement with the literature [61, 62, 64].

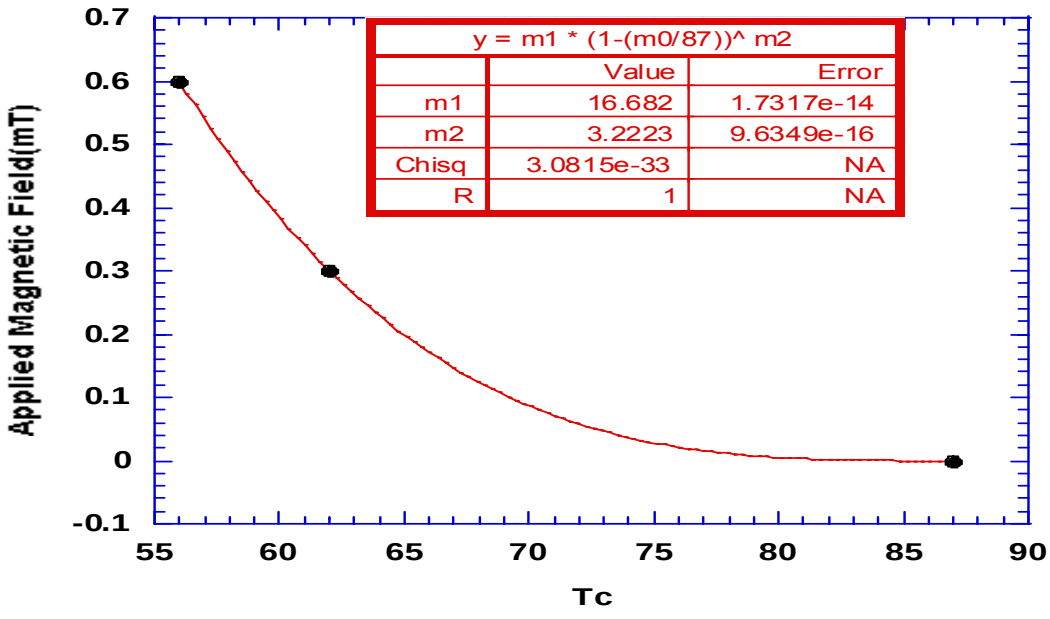

Figure 6.3.5: Activation energies as a function of the critical temperature T_c for 0.0005 Sm.

6.4. I-V (Critical Current vs. Potential Diffrence) Results

Next, critical current densities of the samples were measured in liquid nitrogen and the results are displayed in Fig. 6.4.1 It was found that the critical current densities of the samples decrease sharply from 100 mA/cm^2 to 25 mA/cm^2 with increasing Sm concentration between x = 0.0 and 0.1 [42].

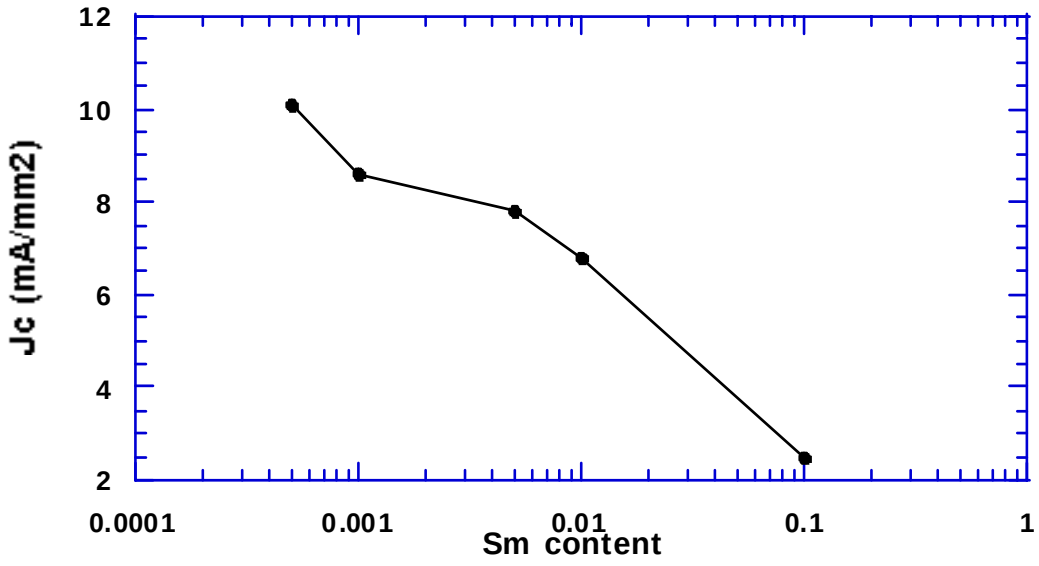

Figure 6.4.1: Critical current densities versus Sm content.

6.5. R vs. H (Resistance as a Function of Applied Magnetic Field) Results

Finally, we want to investigate the resistance dependence of applied magnetic field which changes 0 Tesla to 0.6 Tesla. As we have seen from the graphs, when the magnetic field increases, electrical resistance inreased up to a value significantly and then it continues to increase slightly which is shown in Fig. 6.5.1 and 6.5.2. It is concluded that when the magnetic field increased, pinning centers starts to move and they applied pinning force (lorentz force) to the charge carriers, so this phenomena has the resistivity increased.

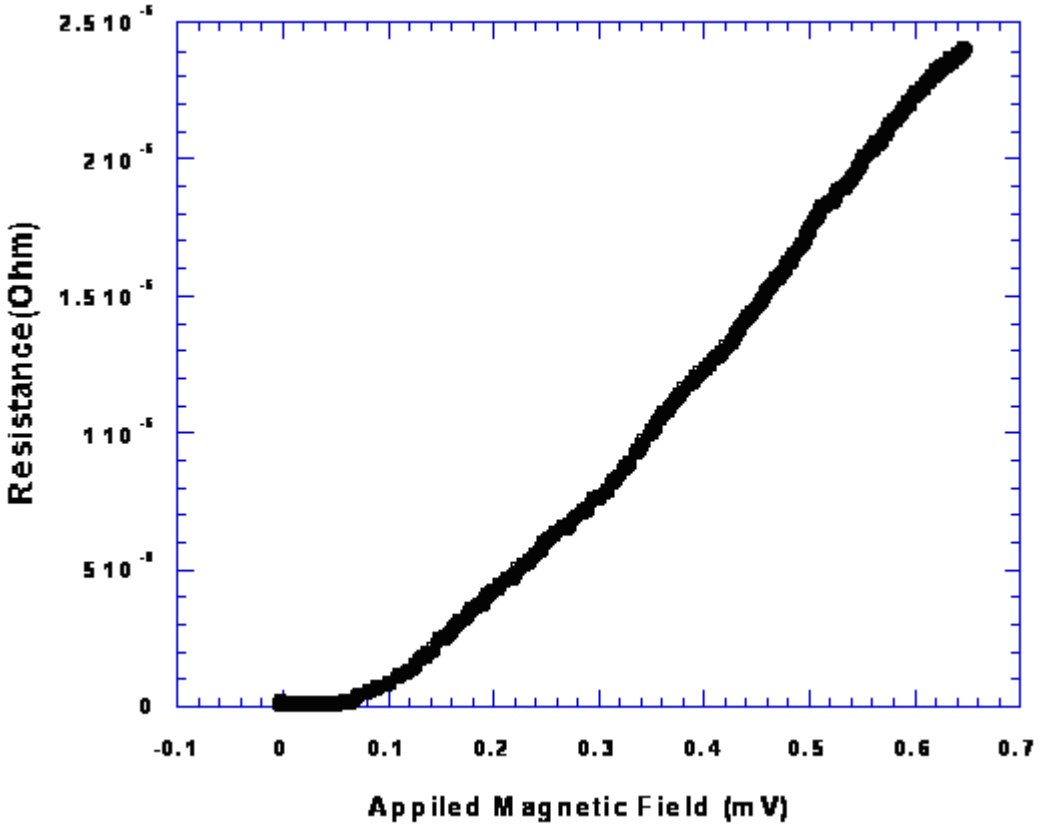

Figure 6.5.1: Resistance as a fuction of Applied magnetic field for 0.001 Sm doped sample with dc current 10mA at 50K.

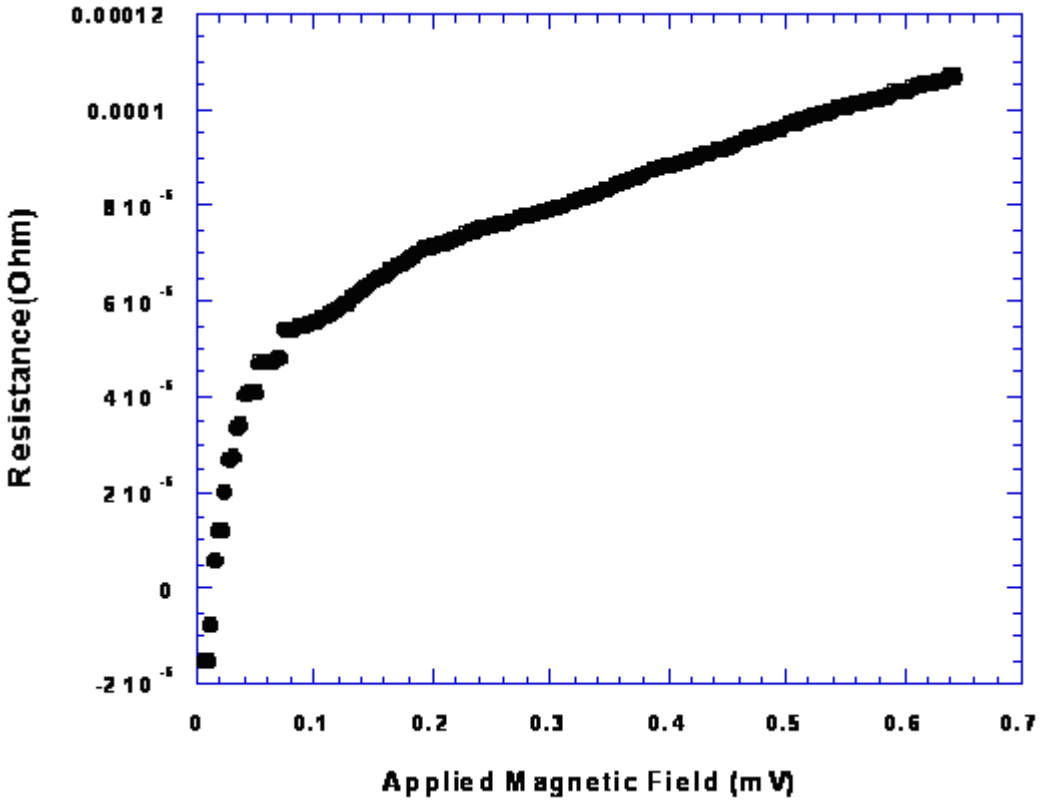

Figure 6.5.2: Resistance as a fuction of Applied magnetic field for 0.0005 Sm doped sample with dc current 10mA at 75K.

CHAPTER 7

CONCLUSION

We have investigated the effect of the partial substitution of Ca by Sm in the mixed and normal state on the activation energy, the irreversibility line (or temperature), and the inter- and intragrain properties of Bi-2223 superconductor using electrical resistivity as a function of temperature and magnetic field. The Sm → Ca substitution in Bi(Pb)SrCaCuO system decreased the J_c, T_c of the sample. The critical temperatures T_c were found to be 107K and 45K for the pure and the Sm-doped samples, respectively. The temperature dependence of the electrical resistivity is linear in the normal state. The residual resistivity increases with increasing x from zero to 0.1 Sm. The width of intragrain transition increases with increasing external dc magnetic field. Activation energy is obtained from Arrhenius plot at different magnetic fields. It was observed that the activation energies are proportional to lnH or H^{-1} for both samples. The irreversibility line is obtained from the zero-resistivity temperature in external dc magnetic field. The behavior of the irreversibility line can be described quite well by the power law relation (see Eq. 6.3.2).

REFERENCES

[1] Kittel, C., Introduction to Solid State Physics, John Wiley & Sons Inc. (1986).

[2] Meissner, W.Ochsenfeld, R., **132** (1933) 931-935.

[3] Bednorz, J.G., Muller, K.A. Possible High T_c Superconductivity in the Ba-La-Cu-O System, Z.Phys, **64** (1986) 189-193.

[4] Jorgensen, J.D., Schutterler, H.B., Hinks, D.G., Capone, D.W., Lattice Instability and High T_c Superconductivity in $La_{2-x}Ba_xCuO_4$, Phys.Rev.Lett.,**58**,**10** (1987) 1024-1027.

[5] Cava, R.J.,Van Dover, R.B., Battlog, B., Rietman, E.A., Phys.Rev.Lett., **58**, **4** (1987) 408-410.

[6] Wu, M.K., Ashburn, J.R., Torng, C, Phys.Rev.Lett. **58**, **9** (1987) 908-910.

[7] Grant, P.M., Beyers, M.B., Engler, E.M., Lim, G., Parkin, S.S.P.,Ramirez, M.L., Lee, V.Y., Nazzal, A., Vazquez, J.E. and Sovay, R.J., Phys.Rev.B, **35**, **13** (1987) 7242-7244.

[8] Quadri, S.B., Toth, L.E., Osofsky, M., Lawrence, S., Gubser, D.U., and Wolf, S.A, Phys.Rev.B, **35**, **13** (1987) 7235-7237.

[9] Hwu, S.J., Song, S.N., Thiel, J., Poeppelmeier, K.R., Ketterson, J.B. and Freeman, A.J., Phys.Rev.B, **35**,**13** (1987) 7119-7121.

[10] Tarascon, J.M., Green, L.H., McKinnon, W.R. and Hull, G.W., Phys.Rew.B, **35**, **13** (1987) 7115-7117.

[11] Kikuchi, M., Syono, Y., Tokiwa, A., Oh-Ishi, K., Arai, H., Hiraga, K., Kobayashi, N., Sasaoka, T. and Muto,Y., Jpn.Appl.Phys., **26**, **6** (1987) L1066-L1069.

[12] Michel, C., et al., Z.Phys.B, Condensed Matter **68**, (1987) 421-423.

[13] Maeda, H., Taraka, Y., Jpn.Appl.Phys., **27**, **2** (1988) L209-L211.

[14] Tokano K. Appl.Phys.Lett., **53**,**14** (1988) 1329-1331.

[15] Quidwai, Ansar A,et al., Supercond.Sci.Technol.,**5**, (1992) 602-604.

[16] Kilic, A., Master Thesis, University of Ankara (2000).

[17] Nagamatsu, J., Nakagawa, N., Muranaka, T., Zenitani,Y., Akimitsu, J., Nature **410** (2001) 63-64.

[18] A.C. Rose-Innes and E.H. Rhoderick, Introduction to Superconductivity, Butterworth-Heineman, (1969)

[19] Arhcroft, N.W., Mermin, N.D., Solid State Physics, Holt Rinehart & Winston (1976).

[20] Raymond A. Serway ,Physics For Scientist&Engineers With Modern Physics. Raymond A. Serway James Madison University , Sounders College Pub, (1992)

[21] Omar, M.A., Elementary Solid State Physics, Addison Wesley, (1993).

[22] H. Maeda, Y. Tanaka, M. Fuktomi, T. Asano, Jpn. J. Appl. Phys., Part 2 **27** (1988) L 209.

[23] M. Muralidhar, S. Satyawathi, V. H. Babu, O. Pena, M. Sergent, J. Mater. Sci. Eng. **B20** (1993) 312.

[24] Belenli, İ, D.PHIL. Thesis, Oxford University (1993).

[25] S. Kambe, Y.C. Guo, S.X. Dou, H.K. Liu, Y. Wakahara, H. Madea, K. Kakimoto, M. Yavuz, Supercond. Sci. Technol. **11** (1998) 1061.

[26] M. Pissas, D. Niarchos, C. Cristides, M. Anagnostou, Semicond. Sci. Technol. **3** (1990) 128.

[27] R.K. Nkum, W.R. Datars, Physica C **190** (1992)465

[28] L. Pierre, J. Shneck, D. Morin, J.C. Toledona, J. Primot, C. Daguet, H. Savary, J. Appl. Phys. **68** (1990)2296

[29] Q. Wu, Z. Fu, A. Zhang, J. Huang, D. Tang, P. Yao, S. Chu, S. Yi, X. Rong, X. Cheng, J. Appl. Phys. **71** (1992) 2772.

[30] J.L. Tallon, R.G. Buckley, P.W. Gilberd, M.R. Presland, Physica C **158** (1989) 247.

[31] V.P.S Awana, S.K. Agarwal, R. Ray, S. Gupta, A.W. Narlikar, Physica C **191** (1992) 43.

[32] K. N. Kishore, M. Muralidhar, V. H. Babu. Physica C **204** (1993) 299.

[33] S. Kambe, Y.C Guo, S.X. Dou, H. K. Liu, Y. Wakahara, H. Maeda, K. Kakimoto, M. Yavuz Supercond. Sci. and Tech. **11** (1998) 1061.

[34] S. Kambe, Y.C Guo, S.X. Dou, H. K. Liu Proc. R. Soc. London **96** (1996) 454.

[35] K. N. Kishore, S. Satyawathi, V. H. Babu, O. Pena, Mater Sci. Eng. B38 **(1996) 267.**

[36] K. N. Kishore, S. Satyawathi, V. H. Babu, O. Pena, M. Muralidhar, M. Sergent, F. Beniere, Status Solidi A **143** (1994) 101.

[37] K. N. Kishore, S. Satyawathi, V. H. Babu, M. Muralidhar, Appl. Supercond. **3** (1995) 267.

[38] D. Rama Sita, R. Signh , Physica C **296** (1998) 21-28.

[39] R. Singh, D.R. Sita, Physica C **312** (1999) 289-298.

[40] Z.W.Zhao, S.L. Li, H. H. Wen, X. G. Li , Physica C **391** (2003) 169-177.

[41] Mehmet Ali Aksan, Mehmet Eyüphan Yakıncı, Journal of Alloys And Compounds **385** (2004) 33.

[42] Cabir Terzioğlu, Mustafa Yılmazlar, Özgür Öztürk, Ekrem Yanmaz, Physica C **423** (2005) 119-126.

[43] P.E. Kazin , V.V. Poltavets , O.N. Poltavets , A.A. Kovalevsky , Yu.D. Tretyakov , M. Jansen , Physica C **324** (1999) 30-38.

[44] D. Milliken , J.H. Ahn, S.X. Dou , Physica C **354** (2001) 183-188.

[45] A. Marifio and J.E. Rodriguez , Physica C **341-348** (2000) 1923-1924.

[46] Z.Y. Jia, H. Tang, Z.Q. Yang, Y.T. Xing, Y.Z. Wang, G.W. Qiao, Physica C **337** (2000) 130-132.

[47] A. Sanchez, J.E. Rodriguez, A. Marino, Physica B **284-288** (2000) 1940-1941.

[48] Mustafa Tepe and Doğan Abukay, Pergamon **108-9** (1998) 613-617.

[49] Vilas Shelke, H.S. Tewari, N.K. Gaur, R.K. Singh, Physica C **300** (1998) 217-224.

[50] N.D. Zhigadlo, V.V. Petrashko, Yu. A. Semenenko, C. Panagopoulos, J.R. Cooper, E.K.H. Salje , Physica C **299** (1997) 327-337.

[51] Sandeep Singh, Physica C **294** (1998) 249-256**.**

[52] Glasso, F.S., Jurnal of Metals **8-10** (1987).

[53] Glasso, F.S., Structure Properties and Preparation of Perovskite Type Compounds, First Edition, Bergamon Press (1969).

[54] Öztürk, Ö, Master Thesis, Abant Izzet Baysal University (2002).

[55] L. Sihan, H. Yusheng, W. Chongde, and S. Zhaohui, Supercond. Sci. Tech., **2** (1989) 145-148.

[56] C.W. Chiu, R.L. Meng, L. Gao, Z. J. Huang, F. Chen, Y. Y. Xuen, Nature (London) **365** (1993) 323.

[57] S. A. Halim, S. A. Kaveideh, S. B. Mohammed, H. Azhan, Mater Chem. Phys. **61** (1999) 251.

[58] H. W. Zandbergen, W. A. Greon, A. Smit, G. V. Tendeloo, Physica C **168** (1990) 426.

[59] G. Ilonca, A. V Pop, Tzuen-Rong Yang, T. Jurcut, C. Lung, G. Stiufiuc, R. Stiufiuc, I. A. Panfilescu. Inorganic Materials **3** (2001) 763-767

[60] A. Madea, T. Yabe, S. Takebayashi, M. Hase, and K. Uchinokura, Physical Review B, **41** (1990) 7.

[61] S. Nezir, S. Çelebi, M. Altuntaş, Alloys Compounds **302** (2000) 235-238.

[62] G. C. Kim, M.Y. Cheon, Y. C. Kim, Physica C **300**(1998) 105-109

[63] N. V. Vo, H. K. Liu and S. X. Dou, Supercond. Sci. Technol. **9** (1996) 104-112.

[64] Z. H. Wang, H. Zhang, Physica C **320** (1999) 218-224.

[65] H. L. Ki, K. Q. Ruan, S. Y. Li, Y. Yu, C. Y. Wang, L.Z. Cao, Physica C **386** (2003) 560-564.